



# Geochemistry and Isotopic Characteristics of Apatite and Zircon From Late Jurassic Granites in the Jiaobei Terrane, East China: Implications for Petrogenesis and Geodynamic Setting

Xiancheng Mao<sup>1,2</sup>, Xin Qu<sup>1,2</sup>, Zhankun Liu<sup>1,2</sup>, Jixian Huang<sup>1,2\*</sup>, Pete Hollings<sup>3</sup>, Peijie Du<sup>4</sup> and Haibin Yang<sup>4</sup>

<sup>1</sup>Key Laboratory of Metallogenic Prediction of Nonferrous Metals and Geological Environment Monitoring, (Ministry of Education), School of Geosciences and Info-Physics, Central South University, Changsha, China, <sup>2</sup>Hunan Key Laboratory of Nonferrous Resources and Geological Hazards Detection, Changsha, China, <sup>3</sup>Department of Geology, Lakehead University, Thunder Bay, Canada, <sup>4</sup>Zhaojin Mining Industry Co., Ltd., Yantai, China

## OPEN ACCESS

### Edited by:

Jean-louis Vigneresse,  
Université de Lorraine, France

### Reviewed by:

Kong-Yang Zhu,  
Zhejiang University, China  
Qiong-Yan Yang,  
China University of Geosciences,  
China

### \*Correspondence:

Jixian Huang  
jxhuang@csu.edu.cn

### Specialty section:

This article was submitted to  
Geochemistry,  
a section of the journal  
Frontiers in Earth Science

**Received:** 07 January 2022

**Accepted:** 16 May 2022

**Published:** 31 May 2022

### Citation:

Mao X, Qu X, Liu Z, Huang J,  
Hollings P, Du P and Yang H (2022)  
Geochemistry and Isotopic  
Characteristics of Apatite and Zircon  
From Late Jurassic Granites in the  
Jiaobei Terrane, East China:  
Implications for Petrogenesis and  
Geodynamic Setting.  
Front. Earth Sci. 10:850440.  
doi: 10.3389/feart.2022.850440

The North China Craton (NCC) was stable for more than 2.0 Gyr before a Jurassic–Cretaceous large-scale lithospheric thinning event, but the geodynamic setting during the early phases (Late Jurassic) of NCC reworking remains controversial. We present new petrological and whole-rock geochemical data, zircon and apatite geochemistry, U–Pb ages, O isotopic data, and Sr–Nd isotopic data for two phases of Late Jurassic granite (Linglong and Luanjiahe) from the Jiaobei terrane, southeastern NCC. LA-ICP-MS zircon U–Pb dating suggests that the Linglong granite formed about 6 Myr earlier than Luanjiahe granite (158 Ma vs 152 Ma), after the inception of the paleo-Pacific plate subduction. High zircon U/Yb ratios, high  $\delta^{18}\text{O}$  values [ $7.89 \pm 0.10\text{‰}$  to  $7.67 \pm 0.14\text{‰}$  ( $2\sigma$ )], and inherited zircon age spectra, as well as high apatite F/Cl ratios and Sr–Nd isotopic compositions, suggest that the Linglong and Luanjiahe granites formed by partial melting of ancient thickened lower continental crust of the NCC and Yangtze Craton. Magma evolution modelling based on Rb and Rb/Nb data suggests a similar decoupled assimilation-fractional crystallization process for the generation of Linglong and Luanjiahe granite but with different assimilation degrees. The water contents of parental magma evaluated by using whole-rock Ba, Sr and apatite F, Cl data indicate that the Linglong granite was formed in a relatively water-rich environment than Luanjiahe. This is consistent with the presence of amphibole and minor negative Eu anomalies in the Linglong granite, as water input can promote amphibole fractionation and suppresses plagioclase crystallization. Considering the similar magma sources but distinct water contents of the granites, and the oblique Paleo-Pacific plate subduction setting in the Late Jurassic, the fluids were likely released from the ocean plate beneath a stacked thickened crust. Since the earliest mafic dikes (OIB-type) in the NCC are coeval with the Luanjiahe granite, we suggest that the lower water contents of the Luanjiahe granite were associated with roll-back that resulted in an increasing distance from slab to continental crust. Such a

tectonic transition from subduction compression (158 Ma) to initial extension (152 Ma) in the Late Jurassic perhaps possibly marks the beginning of the reworking of the NCC.

**Keywords:** granite petrogenesis, accessory mineral geochemistry, paleo-pacific subduction, jiaobei terrane, craton reworking

## INTRODUCTION

The North China Craton (NCC) is an Archean craton that was stable in the Neoproterozoic to Paleoproterozoic with a thick (>200 km) lithosphere (Menzies et al., 1993; Kusky et al., 2007; Zhang et al., 2017) but underwent reworking in the Jurassic–Cretaceous (Rudnick et al., 2004; Wu et al., 2005; Kusky et al., 2007; Zhu et al., 2012). During the Jurassic–Cretaceous, the reworking of the NCC involved a significant lithospheric thinning, losing at least 75–80 km crust, that was associated with intense magmatism, as

evidenced by the presence of large-scale Late Jurassic–Cretaceous granite and mafic dikes (Zhai et al., 2007; Yang J.-H. et al., 2008; Zhang, 2012; Deng et al., 2017). Previous research into the deep Jurassic lithosphere and related granitoid petrogenesis are the subjects of debate. Several studies have linked Jurassic magmatism to asthenospheric upwelling caused by sinking/roll-back of the paleo-Pacific plate (e.g., Jiang Y.-H. et al., 2010; Yang et al., 2012; Ma et al., 2013), while others proposed that the granites formed as a result of the far-field influence of oblique subduction of the paleo-Pacific plate (e.g., Liu et al., 2019; Wu H. J. et al., 2020). This debate has hindered the

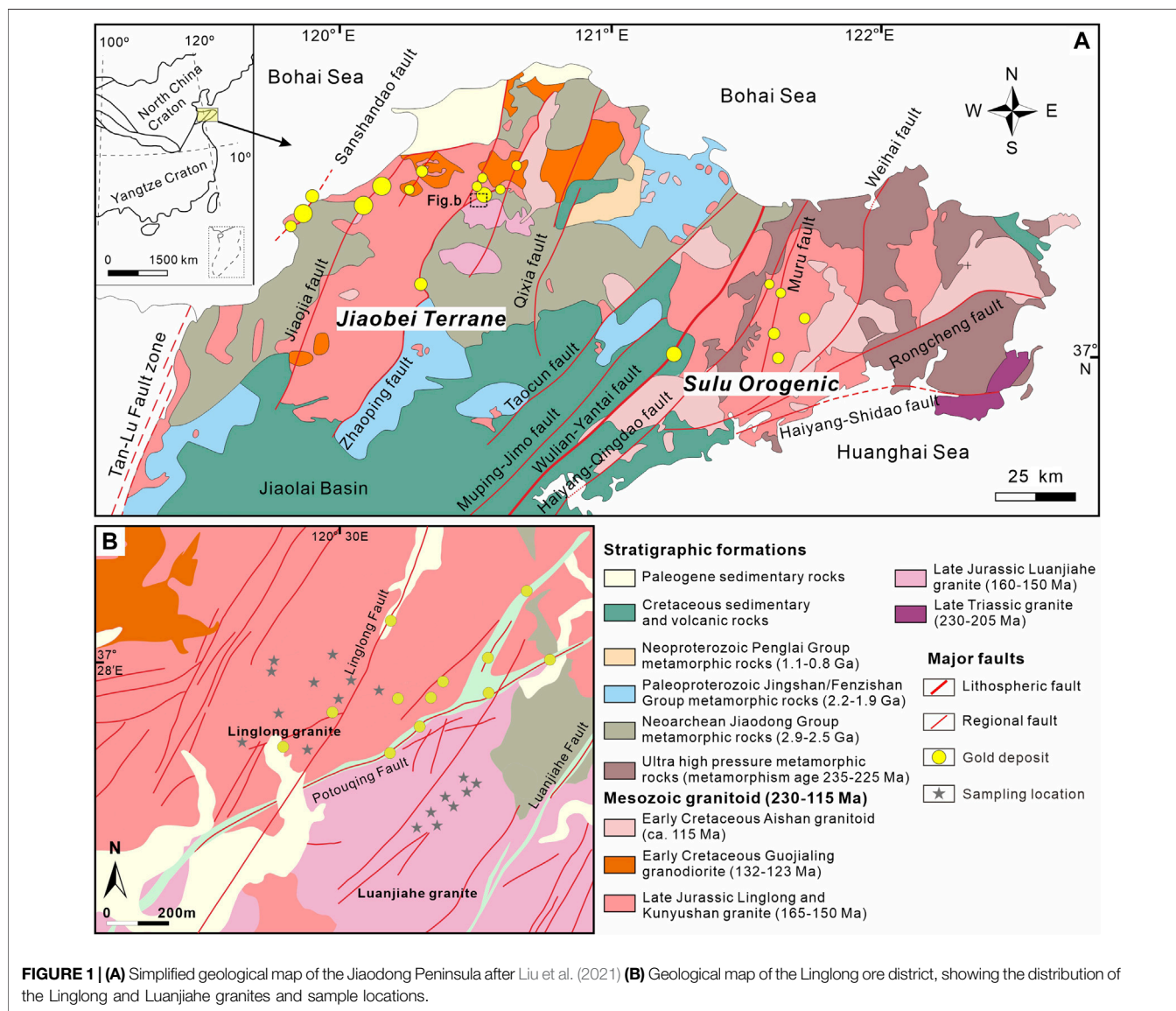


**FIGURE 1 | (A)** Simplified geological map of the Jiaodong Peninsula after Liu et al. (2021) **(B)** Geological map of the Linglong ore district, showing the distribution of the Linglong and Luanjiahe granites and sample locations.

understanding of the lithospheric evolution during the initiation of the reworking of the North China Craton.

The Jiaobei terrane, located on the southeastern margin of the NCC, hosts abundant Late Jurassic–Cretaceous granitoids and large numbers (>200) of Cretaceous gold deposits (**Figure 1A**; Tan et al., 2012; Deng et al., 2020). Two Late Jurassic granitoids, Linglong and Luanjiahe, have been recognized in the Jiaobei terrane (**Figure 1**; Yang et al., 2012; Li H. et al., 2019). Research into the granite petrogenesis has led to models that proposed a similar origin of the partial melting of lower crust for the two granites (Hou et al., 2007; Jiang N. et al., 2010; Yang et al., 2012; Yang et al., 2017). However, field observations show that the Luanjiahe granite intrudes into the Linglong granite and there are distinct differences in mineral assemblages (e.g., biotite, amphibole and feldspar) and textures. These differences suggest there may have been different magmatic processes during the Late Jurassic, which likely provide insights into the geodynamic evolution of NCC.

Zircon and apatite are common accessory minerals in the granite that have been utilized to investigate magmatic and tectonic processes (Hughes and Rakovan, 2015; Andersson et al., 2019; Xing et al., 2021). The composition of zircon and apatite can provide important information on the environment of magma crystallization (Belousova et al., 2002; Hoskin and Schaltegger, 2003), melt volatiles (Scott et al., 2015), the temperature of formation (Ferry and Watson, 2007), redox state (Ballard et al., 2002; Trail et al., 2015; Xing et al., 2021) and sources of the parental magma (Cao et al., 2012; Li et al., 2018). Here, we present petrological observations, zircon and apatite chemistry, zircon U–Pb age and O isotope data, apatite Sr–Nd isotope data, and whole-rock geochemical data. These results provide new constraints on the magma source and petrogenesis of the Late Jurassic Linglong and Luanjiahe granitoids, leading to further understanding of the tectonic evolution of the Jiaobei terrane to decipher the lithospheric dynamics during the initiation of the reconstruction of the NCC.

## GEOLOGICAL BACKGROUND

The Jiaodong Peninsula is divided into two major tectonic units by the Wulian-Yantai Fault: the Jiaobei terrane of the NCC in the west and the Sulu orogenic belt of the Yangtze Craton in the east (**Figure 1A**; Zhai et al., 2000; Tan et al., 2012). Precambrian metamorphic rocks form the basement of the Jiaobei terrane, consisting of the Archean Jiaodong Group (tonalite-trondhjemite-granodiorite (TTG) and amphibolites), the Paleoproterozoic Jingshan/Fenzishan, and the Neoproterozoic Penglai Group (Jiang N. et al., 2010; Liu et al., 2021). The protolith of the Jiaodong Group was formed by a series of magmatic processes, including crustal thickening at ca. 2.9 and 2.7 Ga and subduction at ca. 2.5 Ga (Liu et al., 2021). The overlying Jingshan and Fenzishan Groups are in unconformable contact with the Jiaodong Group and comprise mostly schist, gneiss, calcareous silicate, marble, minor granulites, and amphibolite, with the ages of 1.8–2.5 Ga (Ma et al., 2013). The primary lithologies of the Penglai Group include low-grade metamorphic rocks such as marble, slate, quartzite, phyllite, and marl (Li X.-H. et al., 2019; Liu et al., 2021).

The Precambrian basement of the Sulu belt is dominated by ultrahigh-pressure and low-temperature metamorphic assemblages, such as granitic gneiss, coesite-bearing eclogite, siliceous rocks (Wang et al., 2021), the protoliths of which are 780–740 Ma in age (Zhao et al., 2016; Yang et al., 2017), and minor eclogite, amphibolite, and granulite with ages of 2.0–1.8 Ga (Zhao et al., 2016).

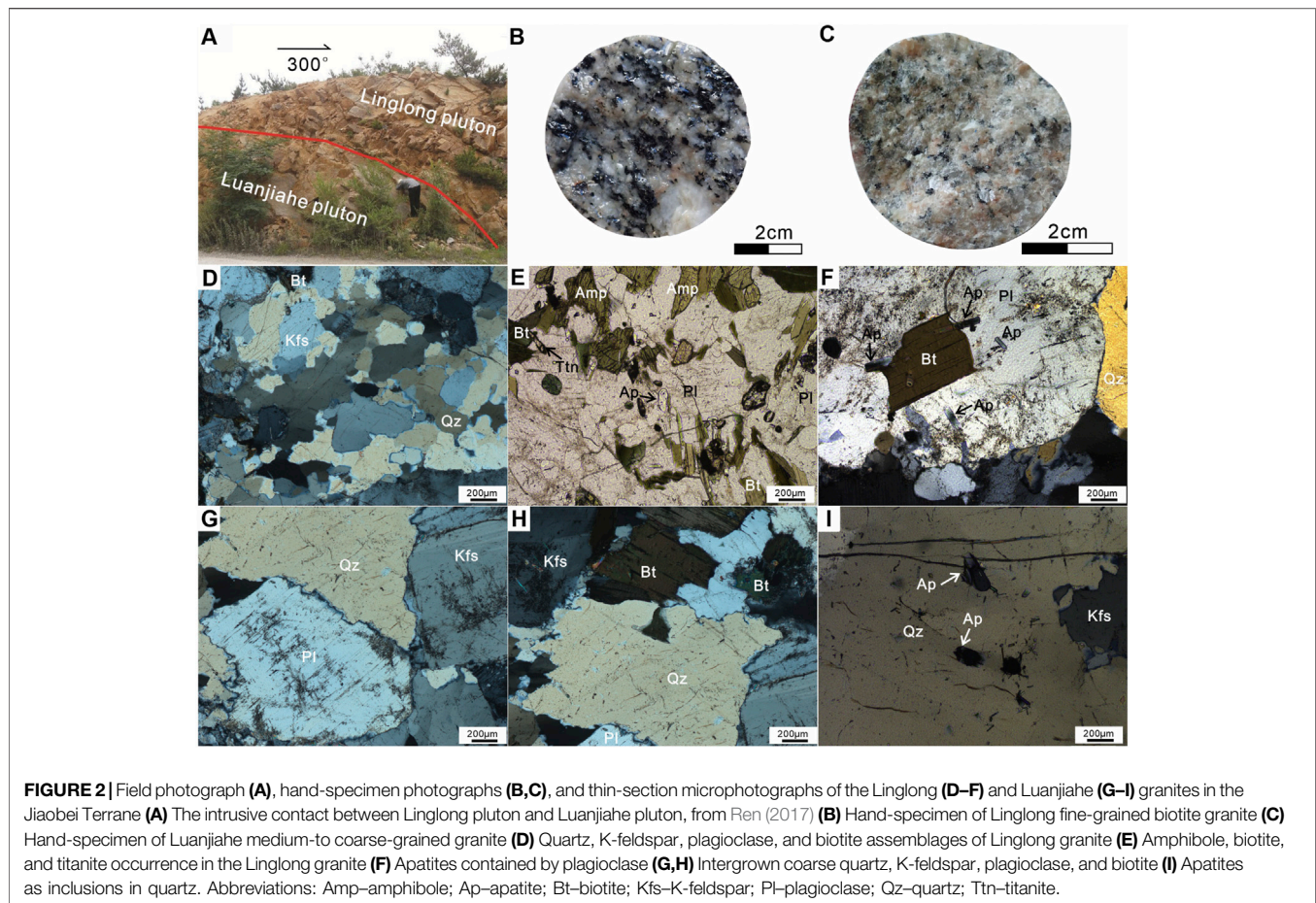
The Mesozoic magmatism is dominated by the Late Jurassic (160–146 Ma; Yang et al., 2017) and Early Cretaceous granites (130–120 Ma; Tang et al., 2014). Late Triassic granites (225–205 Ma; Ma et al., 2013) occur only in the east of the Jiaodong Peninsula, whereas the Late Jurassic and Early Cretaceous granites are more widespread (**Figure 1A**; Liu et al., 2021). The Late Triassic synorogenic granites and post-orogenic high-alkali feldspar syenites in the Sulu orogenic belt were formed during the north-south trending collision of the NCC with the Yangtze craton (Zhai et al., 2000). The Late Jurassic magmatism is the most extensive event in the Jiaodong Peninsula and includes the Linglong and Luanjiahe granites (Hou et al., 2007; Ma et al., 2013). These Late Jurassic granites intruded into the metamorphic basement rocks of the Jiaobei terrane and Sulu orogenic belt (Ma et al., 2013). The Linglong and Luanjiahe granites occur as a band along the NNE-trending detachments in the northwest Jiaodong Peninsula (**Figure 1A**; Zhang et al., 2010b) and were intruded by Early Cretaceous Guojialing-type and Aishan-type granodiorite (Hou et al., 2007). The Early Cretaceous Guojialing and Weideshan granodiorites (130–120 Ma; Tang et al., 2014) have been interpreted to have formed by the crystallization of a magma derived from a mix of crust and mantle (Wu et al., 2005; Tang et al., 2014). In addition, there are many NNE-NE trending Cretaceous mafic dikes (e.g., lamprophyre and dolerite) in the Jiaodong Peninsula.

## SAMPLES AND ANALYTICAL METHODS

### Samples

In this study, we collected ten fresh Linglong granite samples and eight Luanjiahe samples in the northwest of the Jiaodong Peninsula (**Figure 1B**). The Luanjiahe pluton often invaded into the Jiaodong Group metamorphic rocks and/or Linglong pluton, showing an intrusive contact relationship (**Figure 2A**).

The Linglong granite consists mainly of fine-grained biotite granite with local gneissic textures and is grey in hand-specimen (**Figure 2B**). The main mineral assemblages of the Linglong granites consist of quartz (20–30 vol%), K-feldspar (30–40 vol%), plagioclase (25–30 vol%), biotite (6–10 vol%) and amphibole (3–5 vol%), with minor accessory zircon, titanite, garnet, and apatite (**Figures 2D–F**). The Luanjiahe granite has a medium-to coarse-grained texture and is pale red in hand-specimen (**Figure 2C**). The main mineral assemblages of the Luanjiahe granites consist of quartz (25–40 vol%), K-feldspar (35–45 vol%), and plagioclase (30–45 vol%), with minor accessory zircon, garnet, and apatite (**Figures 2G–I**). Compared to the Linglong granites, the Luanjiahe granites contain more quartz and plagioclase, with no amphibole and little biotite (~2 vol%).



## Whole-Rock Geochemistry

Major and trace elements were determined by XRF and ICP-MS respectively at ALS Chemex Co Ltd, Guangzhou, China. Samples were firstly pulverized to 200 mesh under freezing temperature conditions and the composition of the major elements was determined by XRF. Standards GBW07105 and ARM-4 were used as reference materials for monitoring the major elements. After dissolution with lithium borate, trace elements were measured by ICP-MS. Reference standards OREAS-120 and OREAS-100a were used to monitor trace elements during analysis. The analytical accuracy for major and trace elements is better than 3% and 10%, respectively.

## EPMA Analysis of Apatite

The major element analysis of apatite was undertaken with a JEOL JXA-8230 Electron Probe Microanalyzer (EPMA) with five wavelength-dispersive spectrometers (WDS) at Wuhan Microbeam Analysis Technology Co., Ltd. The accelerating voltage was 15 kV, the accelerating current was 5 nA, and the spot diameter was 20–40  $\mu\text{m}$  for quantitative WDS analysis. The peaks of Na, Sr, Ca, Cl, S, F, and P elements were measured for 10 s. The high-energy and low-energy backgrounds had measurement times that were half of the peak measurement duration. The specimens used for the test elements were jadeite (Na), celestite (Sr), NaCl (Cl), barite (S), fluorite (F),

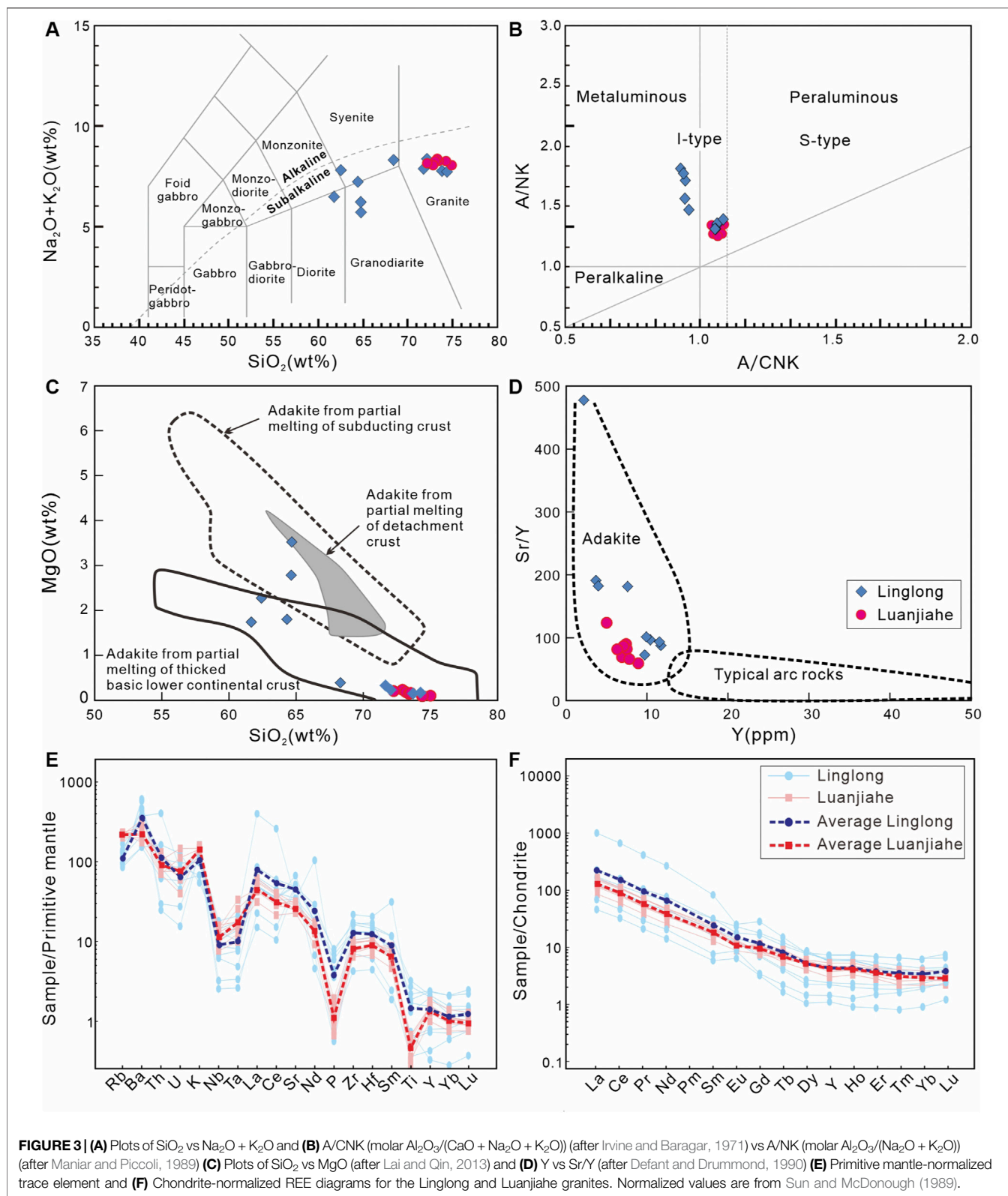
apatite (P, Ca). The detection limit was  $\sim 100$  ppm for Cl,  $\sim 200$  ppm for Ca, Na, P, and S, and  $\sim 200$  ppm for F and Sr, with an accuracy of  $\pm 1.5\%$ .

## LA-ICP-MS Analysis of Zircon and Apatite

Zircon and apatite LA-ICP-MS trace elements and U–Pb geochronology analyses were measured with a Teledyne Photon Machines Analyte He Excimer 193 nm laser ablation system, equipped with an Analytik Jena PlasmaQuant MS Ellite at the Central South University, China. Samples were placed in a sealed ablation chamber which was flushed with a combination of high-purity Ar (13.5 L/min) and He gas (1.1 L/min) at a constant rate. The laser repetition rate was  $\sim 5$  Hz, and the spot size was 50  $\mu\text{m}$ . Each spot was subjected to a 15–25 s background acquisition followed by a 35–45 s sample ablation. External standards for U–Pb dating and trace element calibration were zircon 91,500 and glass NIST610, respectively. The Si and Ca (determined by EPMA) were used as the internal standard for zircon and apatite, respectively. Data were processed using the GLITTER program (Griffin et al., 2008).

## SIMS O Isotope Analysis of Zircon

Zircon oxygen isotope analyses were performed with a CAMECA IMS 1280-HR SIMS at the State Key Laboratory of Isotope Geochemistry, Guangzhou Institute of Geochemistry. Detailed



methods are described in (Li et al., 2009). The principal ion stream employed was  $^{133}\text{Cs}$  with an intensity of about 2 nA, which was focused into a beam spot of around  $10\ \mu\text{m}$  size after

passing an accelerating voltage of 10Kv. The secondary ion signal was collected by scanning an area of about  $20\ \mu\text{m}$  size on the sample surface in a raster scanning mode. The Penglai zircon

standard ( $\delta^{18}\text{O} = 5.31\text{‰} \pm 0.10\text{‰}$ ) was used to calibrate the instrument mass fractionation. The measured  $\delta^{18}\text{O}/^{16}\text{O}$  ratios were adjusted using the Vienna Standard Mean Ocean Water ( $V_{\text{SMOW}}$ ) composition ( $\delta^{18}\text{O}/^{16}\text{O} = 0.0020052$ ). The corrected  $\delta^{18}\text{O}$  readings were reported in conventional per-mil notation with  $2\sigma$  error.

## LA-MC-ICP-MS Sr-Nd Isotope Analysis of Apatite

The apatite Sr-Nd isotope analysis was carried out at Beijing Createch Testing Technology Co., Ltd. utilizing a Neptune Plus MC-ICP-MS coupled with a RESOLUTION SE 193 nm UV-ArF excimer laser ablation system. The isotope data were obtained by multiple static acquisitions using nine Faraday collectors in low-resolution mode. The spot ablation was performed using a 50–100  $\mu\text{m}$  spot with an energy density of  $8\text{ J/cm}^2$  and a laser pulse frequency of 10 Hz. The standard data-gathering cycle includes a 10 s Kr gas background acquisition and a 20 s measurement. The detailed Nd and Sr isotope methods are presented in Yang Y. et al. (2008) and Yang et al. (2009), respectively. The mass fractionation of Nd and Sr isotopes was estimated using the exponential law and adjusted using  $^{144}\text{Nd}/^{146}\text{Nd} = 1.385233$  and  $^{88}\text{Sr}/^{86}\text{Sr} = 8.375209$ . The Durango apatite was used as a standard. Seventeen spots of Durango yielded average  $^{143}\text{Nd}/^{144}\text{Nd} = 0.512465 \pm 26$  (2SD),  $^{145}\text{Nd}/^{144}\text{Nd} = 0.348407 \pm 26$  (2SD) and 18 spots of Durango yielded average  $^{84}\text{Sr}/^{86}\text{Sr} = 0.0566 \pm 21$  (2SD),  $^{87}\text{Sr}/^{86}\text{Sr} = 0.70597 \pm 41$  (2SD). The data for the standard is consistent with the reported  $^{143}\text{Nd}/^{144}\text{Nd}$  ratios of 0.51075–0.512497 and  $^{145}\text{Nd}/^{144}\text{Nd}$  of 0.3484–0.348419 as well as  $^{84}\text{Sr}/^{86}\text{Sr}$  of 0.05560–0.05667 and  $^{87}\text{Sr}/^{86}\text{Sr}$  of 0.70500–0.70641 (<http://georem.mpch-mainz.gwdg.de>).

## RESULTS

### Whole-Rock Geochemistry

Major and trace element data are shown in **Supplementary Table S1**. The Linglong and Luanjiahe granites have  $\text{SiO}_2$  contents of 61.65–73.66 wt% and 72.16–74.89 wt%,  $\text{Al}_2\text{O}_3$  contents of 14.51–17.07 and 13.68–14.74 wt%, and total alkali ( $\text{K}_2\text{O} + \text{Na}_2\text{O}$ ) contents of 5.66–8.32 wt% and 7.98–8.29 wt%, whereas the compositions of the Linglong granite are more variable. Chemically, the two granite units belong to the subalkaline series (**Figure 3A**) and are metaluminous to weakly peraluminous (**Figure 3B**). Their Mg# ( $\text{Mg\#} = 100 \text{ Mg}^{2+}/(\text{Mg}^{2+} + \text{Total Fe}^{2+})$ ) values are low, ranging from 18 to 59 (mean 37) and 14–22 (mean 18; **Supplementary Table S1**), but the MgO contents of the Linglong granite are higher than those of Luanjiahe (**Figure 3C**).

Generally, the Sr/Y ratios of the Linglong and Luanjiahe granites are relatively high (**Figure 3D**). All granite samples show enrichment in large-ion lithophile elements (LILE; e.g., Ba, Rb, Th, and U) and depletion in high-field strength elements (HFSE; e.g., Nb, Ta, Zr, Hf, and Ti; **Figure 3E**). The total REE contents of the Linglong granites are highly variable ( $\Sigma\text{REE} = 41\text{--}888$  ppm, mean 208 ppm), and higher than Luanjiahe

(83–151 ppm, mean 123 ppm). Both the granites have similar chondrite-normalized REE patterns with enrichment in light rare earth elements (LREE) and relative depletion in heavy rare earth elements (HREE), but the Linglong granite has a higher LREE enrichment ( $(\text{La}/\text{Yb})_{\text{N}} 22.8\text{--}260.3$  vs  $28.9\text{--}76.3$ ; **Figure 3F**). The Eu anomalies ( $\text{Eu}/\text{Eu}^* = \text{Eu}_{\text{N}}/(\text{Sm}_{\text{N}} \times \text{Gd}_{\text{N}})^{0.5}$ ) of the Linglong and Luanjiahe granites are weakly negative to positive ( $\text{Eu}/\text{Eu}^* = 0.53\text{--}1.70$  and  $0.62\text{--}1.03$ ; **Figure 3F**).

### Zircon U–Pb Ages, Trace Elements, and O Isotope

The zircon geochronology, geochemistry, and SIMS O isotope data are shown in **Supplementary Tables 2, 3**. Zircons separated from the Linglong and Luanjiahe granites are prismatic and stubby with a width of  $\sim 200\ \mu\text{m}$  and an aspect ratio of 3:1–3:2. Oscillatory and planar zonation has been observed in CL images (**Figures 4A,B**), and Th/U ratios are relatively high (Linglong 0.16–0.92, mean 0.49; Luanjiahe 0.05–1.02, mean 0.46; **Supplementary Table S2**), consistent with a magmatic origin (Hoskin and Schaltegger, 2003).

The Luanjiahe pluton invaded into the Linglong pluton (**Figure 2A**), suggesting that the Luanjiahe granites formed later than the Linglong granites. Eleven spots were analysed on zircon from sample 199ZK1-10, yielding a concordant age of  $157.5 \pm 3.5$  Ma (MSWD = 0.36), and the weighted mean age was  $158.2 \pm 3.2$  Ma (MSWD = 0.35; **Figure 5A**). Twelve spots of sample 199ZK1-11 define a concordant age of  $157.6 \pm 3.1$  Ma (MSWD = 0.65), and a weighted mean age of  $157.5 \pm 3.5$  Ma (MSWD = 0.60; **Figure 5B**). Zircons from the Luanjiahe granite (LJHZK1-01) yielded a concordant age of  $151.7 \pm 2.1$  Ma (MSWD = 0.80,  $n = 24$ ), and a weighted mean age of  $150.6 \pm 1.6$  Ma (MSWD = 1.5; **Figure 5C**).

The Linglong and Luanjiahe zircons are mostly characterized by enrichment in HREE, negative Eu anomalies (Linglong:  $\text{Eu}/\text{Eu}^* = 0.14\text{--}0.71$ ; Luanjiahe:  $\text{Eu}/\text{Eu}^* = 0.12\text{--}0.60$ ) and strong positive Ce anomalies ( $\text{Ce}/\text{Ce}^* = \text{Ce}_{\text{N}}/(\text{La}_{\text{N}} \times \text{Pr}_{\text{N}})^{0.5}$ ; Linglong:  $\text{Ce}/\text{Ce}^* = 3.83\text{--}471.75$ ; Luanjiahe:  $\text{Ce}/\text{Ce}^* = 1.79\text{--}436.83$ ; **Figure 6A**; **Supplementary Table S2**). Both have high  $\Sigma\text{REE}$  and Y contents and a positive correlation between them (**Supplementary Table S2**). Linglong and Luanjiahe zircons exhibit similar REE patterns. There is a significant divergence between the light and heavy rare earth elements (Linglong:  $\Sigma\text{LREE}/\Sigma\text{HREE} = 0.02\text{--}0.08$ ; Luanjiahe:  $\Sigma\text{LREE}/\Sigma\text{HREE} = 0.01\text{--}0.08$ ), with heavy rare-earth enrichment and light rare-earth depletion, with negative Eu anomalies and positive Ce anomalies (**Figure 6A**).

The  $\delta^{18}\text{O}$  values of Linglong zircons range from 7.52 to 8.36‰, with a weighted average value of  $7.88 \pm 0.10\text{‰}$  ( $2\sigma$ ,  $n = 25$ ; **Supplementary Table S3**), whereas the Luanjiahe zircons have slightly low  $\delta^{18}\text{O}$  values (7.05 to 8.26‰, average  $7.67 \pm 0.14\text{‰}$  ( $2\sigma$ ,  $n = 24$ )).

### Apatite Geochemistry

The major and trace element results are shown in **Supplementary Tables 4, 5**. Apatites separated from the Linglong and Luanjiahe granites are prismatic and stubby with a width of 100–200  $\mu\text{m}$

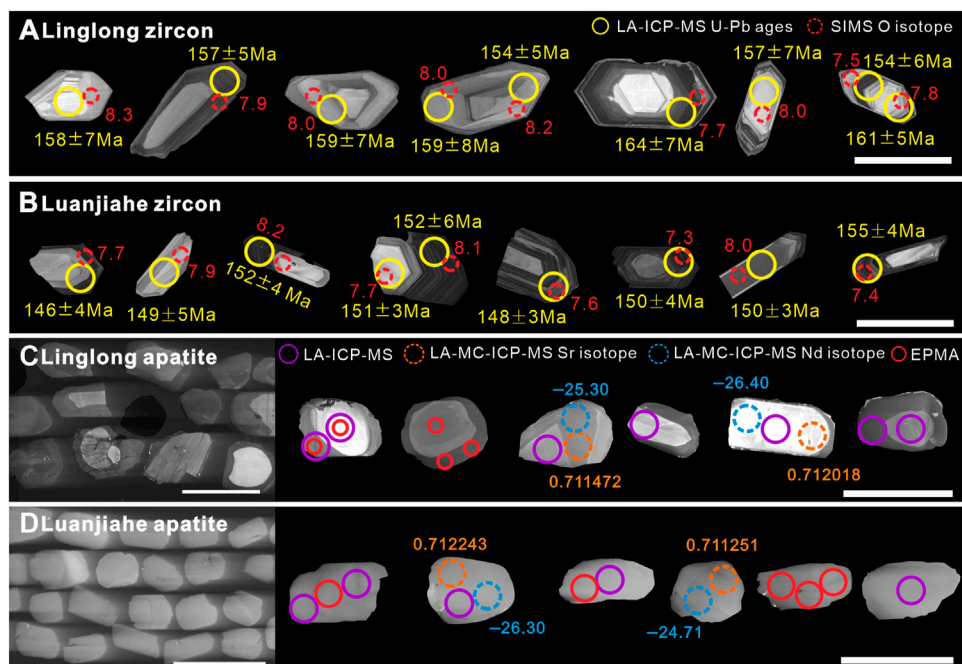


**FIGURE 4 | (A,B)** Cathodoluminescence (CL) images of representative zircons, with the ages and  $\delta^{18}\text{O}$  values given nearby **(C,D)** Phosphorescence effect and Cathodoluminescence (CL) images of representative apatites, with the initial  $^{87}\text{Sr}/^{86}\text{Sr}$  ratios and  $\epsilon_{\text{Nd}}(t)$  values given nearby. The scale bar is 200  $\mu\text{m}$ .

and an aspect ratio of 3:1–3:2 (Figures 4C,D). The apatite from the Linglong granites has a distinct zonal structure (Figure 4C), whereas the Luanjiahe apatite is homogeneous and has a distinct and strong phosphorescence effect (Figure 4D). The major elements and trace elements of apatite from Linglong vary markedly between the cores and rims. The CaO and P<sub>2</sub>O<sub>5</sub> contents of Linglong and Luanjiahe granites are weakly variable, ranging from 54.7 to 56.2 wt% and 53.8 to 55.6 wt% and 41.2 to 42.9 wt% and 40.9 to 42.4 wt% (Supplementary Table S4), respectively. The SrO, Na<sub>2</sub>O, and SO<sub>3</sub> contents are very low (most lower than 0.1 wt%). The Luanjiahe granite contains high F contents than Linglong (3.46–3.77 wt% vs 2.99–3.73 wt%, mean 3.43 wt% vs 3.72 wt%) and Cl contents of all analyzed apatites are extremely low (mostly lower than 0.1 wt%; Supplementary Table S5), thereby exhibiting a strong negative correlation between F and OH (Figure 7B). The F concentrations in the cores are more enriched than the rims of the Linglong apatites (3.33–3.73 wt% vs 2.99–3.44 wt%; Supplementary Table S4).

The Linglong apatite has relatively high Sr contents of 619–1315 ppm and low Y contents of 77–2169 ppm than Luanjiahe (491–736 ppm vs 1795–4856 ppm; Supplementary Table S4). The Linglong and Luanjiahe apatites show similar flat REE patterns and negligible Ce anomalies, but with different Eu anomalies (Figure 6B). This is also reflected in the cores and rims revealed by CL imaging of the Linglong apatite. The REE, Y, Th, and U concentrations in the cores are more enriched than the rims ( $\Sigma\text{REE} = 1529\text{--}5312$  ppm vs  $323\text{--}2081$  ppm, Y =  $319\text{--}2169$  ppm vs  $76\text{--}902$  ppm, Th =  $5.4\text{--}47$  ppm vs  $0.1\text{--}21.3$  ppm, U =  $3.0\text{--}73$  ppm vs  $0.5\text{--}37$  ppm; Supplementary Table S5) and have stronger negative Eu anomalies ( $\text{Eu}/\text{Eu}^* = 0.23\text{--}0.63$

and 0.70–2.40; Figure 6B). The Luanjiahe apatite has the highest REE contents ( $\Sigma\text{REE} = 4421\text{--}10,599$  ppm) and negative Eu anomalies ( $\text{Eu}/\text{Eu}^* = 0.12\text{--}0.32$ ; Supplementary Table S5).

### Apatite Sr and Nd Isotopic Compositions

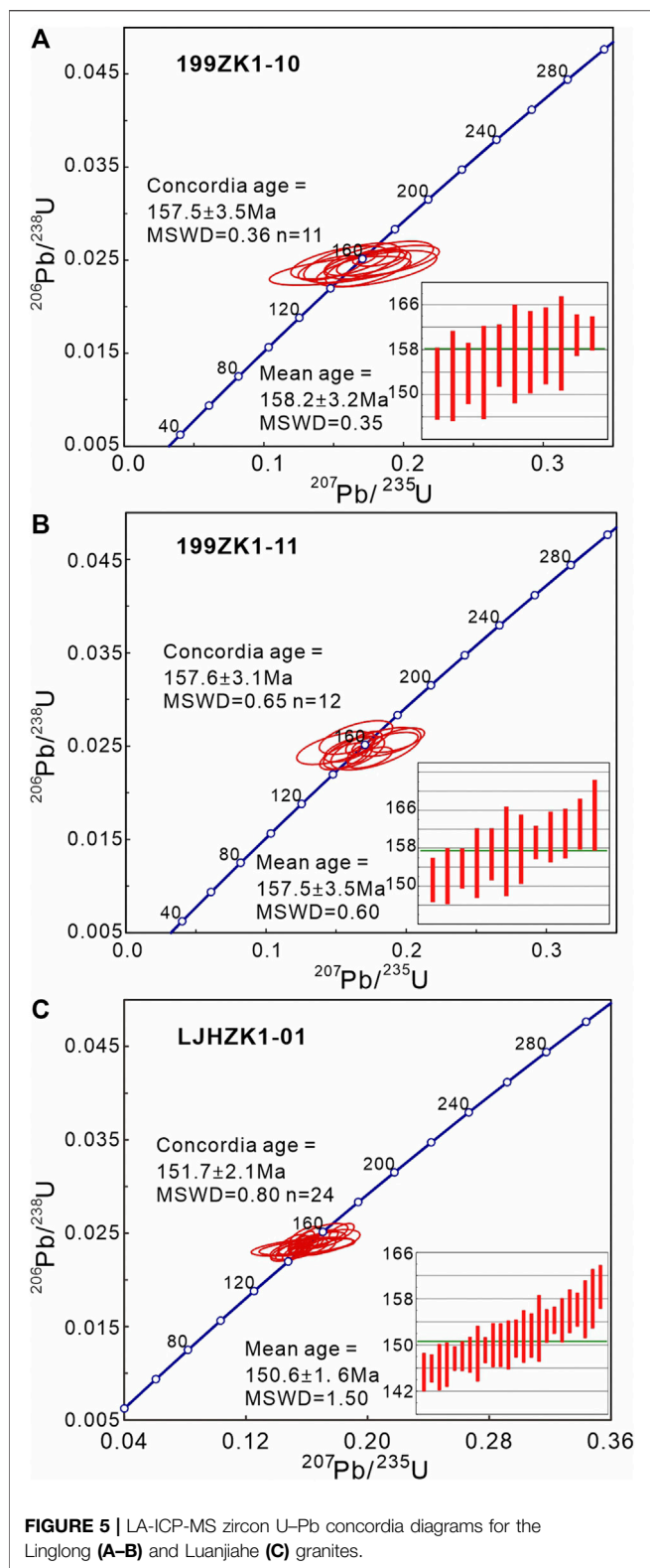
The Sr and Nd isotope data of the Linglong and Luanjiahe apatites are presented in Supplementary Table S6. All analyses of Linglong and Luanjiahe apatites exhibit a tight range of  $^{87}\text{Sr}/^{86}\text{Sr}$  (0.711443–0.714458 and 0.710729–0.712695) and  $^{143}\text{Nd}/^{144}\text{Nd}$  (0.511402–0.511576 and 0.511356–0.511666). The calculated initial  $^{87}\text{Sr}/^{86}\text{Sr}$  ratios and  $\epsilon_{\text{Nd}}(t)$  values are similar in Linglong (mean 0.71233 and  $-26.52$ ) and Luanjiahe apatites (mean 0.71169 and  $-26.15$ ; Supplementary Table S6).

## DISCUSSION

### Identification of Partial Melts From Ancient Continental Crust

The Late Jurassic granites from this study have low Mg#, low Rb/Sr, and metaluminous to slightly peraluminous characteristics, consistent with them having been derived from an intermediate-felsic orthogneiss. New zircon and apatite geochemistry and isotope data provide further constraints on the magmatic sources of the Linglong and Luanjiahe granite.

- 1) The moderate Hf and Y contents and high U/Yb ratios of zircon are consistent with the characteristics of continental zircons (Figure 8; Grimes et al., 2007).



2) Chloride and F have different partition coefficients during magma differentiation so that Cl is enriched in the fluid phase in the mantle, whereas the lithophile affinity of F causes it to

enter the melt phase and be enriched in the crust. Thus, high F/Cl ratios of apatite typically reflect a crustal source (Mathez and Webster, 2005; Webster et al., 2009). Both the Linglong and Luanjiahe apatites have high F/Cl ratios (28–187 and 82–377; **Supplementary Table S4**), suggesting a crustal source (Boudreau and Kruger, 1990; Webster et al., 2009).

- 3) The  $\delta^{18}\text{O}$  values of zircon from the Linglong and Luanjiahe samples range from 7.52 to 8.36‰ and 7.05 to 8.26‰, similar to ancient continental crust and related melts/fluids (**Figure 9**; Yang J.-H. et al., 2008). The crust-like  $\delta^{18}\text{O}$  values in zircon, combined with the strongly negative  $\epsilon_{\text{Hf}}(t)$  values (**Figure 9**), suggest they formed by melting ancient continental crust. The slightly lower  $\delta^{18}\text{O}$  values of the Luanjiahe zircon may reflect a minor contribution of residual Yangtze craton given its low  $\delta^{18}\text{O}$  values (–0.4 to 5.1‰; Jiang N. et al., 2010).
- 4) The  $\epsilon_{\text{Nd}}(t)$  and initial  $^{87}\text{Sr}/^{86}\text{Sr}$  values of Linglong and Luanjiahe apatites plot between the fields of the lower crust of the Yangtze craton and the upper crust of the NCC, suggesting both may have acted as sources for the granite magmas (**Figure 10**). This is supported by the occurrence of Neoproterozoic, Neoproterozoic, and Triassic inherited zircons in the Linglong and Luanjiahe granites (**Supplementary Figure S1**), which coincide with the formation time of the NCC and Yangtze craton (2.7–2.9 Ga, ~2.5 Ga, ~1.9 Ga) or the metamorphic age (~200 Ma) of the Sulu orogenic belt (**Supplementary Figure S1**).

Taken together, the Late Jurassic granitic magma in the Jiaobei terrane was dominantly formed by partial melting of the ancient continental crust of the NCC with a minor contribution from the Yangtze Craton.

## Magma Nature and Evolution of Late Jurassic Granites

### Magma Oxidation and Hydration States

Cerium and Eu both have two valence states (i.e.  $\text{Ce}^{3+}$  vs  $\text{Ce}^{4+}$  and  $\text{Eu}^{2+}$  vs  $\text{Eu}^{3+}$ ). Zircon prefers to incorporate  $\text{Eu}^{3+}$  and  $\text{Ce}^{4+}$  in their lattice, whereas apatite prefers  $\text{Eu}^{3+}$  and  $\text{Ce}^{3+}$  (Drake, 1975; Ballard et al., 2002; Belousova et al., 2002; Cao et al., 2012). Zircon and apatite cerium and Eu anomalies have long been used to characterize the oxidation status of host rocks (e.g., Trail et al., 2011; Cao et al., 2012; Trail et al., 2015; Du et al., 2019; Xing et al., 2021). Due to the influence of mineral fractionation and element incorporation on element partitioning (Bruand et al., 2014; Wang et al., 2020), the correlation between Ce and Eu anomalies is more suitable for determining the oxidation state than single anomalies (Cao et al., 2012; Du et al., 2019). The  $\text{Ce}/\text{Ce}^*$  and  $\text{Eu}/\text{Eu}^*$  of the Linglong and Luanjiahe zircons ( $\text{Ce}/\text{Ce}^* = 3.83\text{--}471.75$  and  $\text{Ce}/\text{Ce}^* = 1.79\text{--}436.83$ ,  $\text{Eu}/\text{Eu}^* = 0.14\text{--}0.71$  and  $0.12\text{--}0.60$ ; **Supplementary Table S2**) have no significant co-variation (**Figure 11A**). A similar trend between  $\text{Ce}/\text{Ce}^*$  and  $\text{Eu}/\text{Eu}^*$  also exists in the apatite data ( $\text{Ce}/\text{Ce}^* = 0.98\text{--}1.09$  and  $0.98\text{--}1.06$ ,  $\text{Eu}/\text{Eu}^* = 0.32\text{--}2.40$  and  $0.12\text{--}0.32$ ; **Figure 11B**; **Supplementary Table S5**), where Luanjiahe apatites have stronger negative Eu anomalies than Linglong apatites owing to the influence of plagioclase (Eu-rich mineral) crystallization.

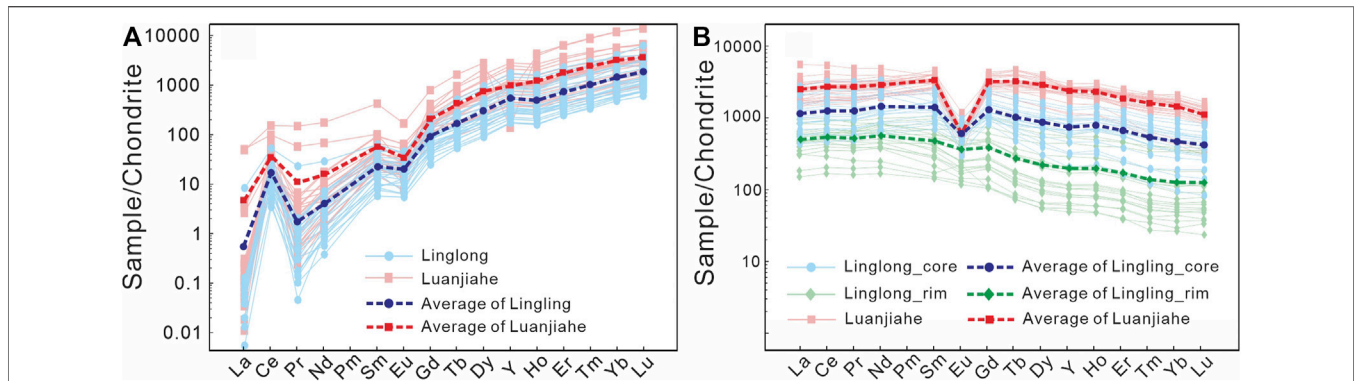


**FIGURE 6 | (A)** Chondrite-normalized REE pattern of zircon **(A)** and apatite **(B)** from Linglong and Luanjiahe granites. Chondrite normalizing values are from Sun and McDonough (1989).

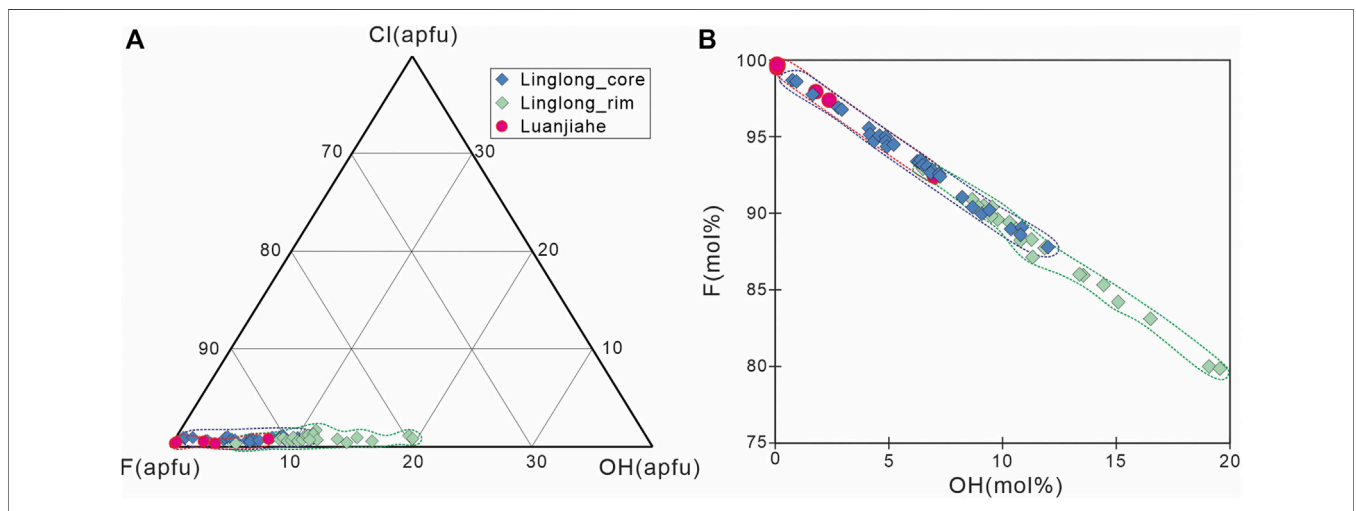


**FIGURE 7 | F-Cl-OH ternary diagram (A)** and F-OH diagram **(B)**. The OH content in apatite is calculated based on the assumption that halogen sites are occupied completely with  $X_F + X_{Cl} + X_{OH} = 1$ , where X is the mole fraction modulus (Piccoli and Candela, 2002).

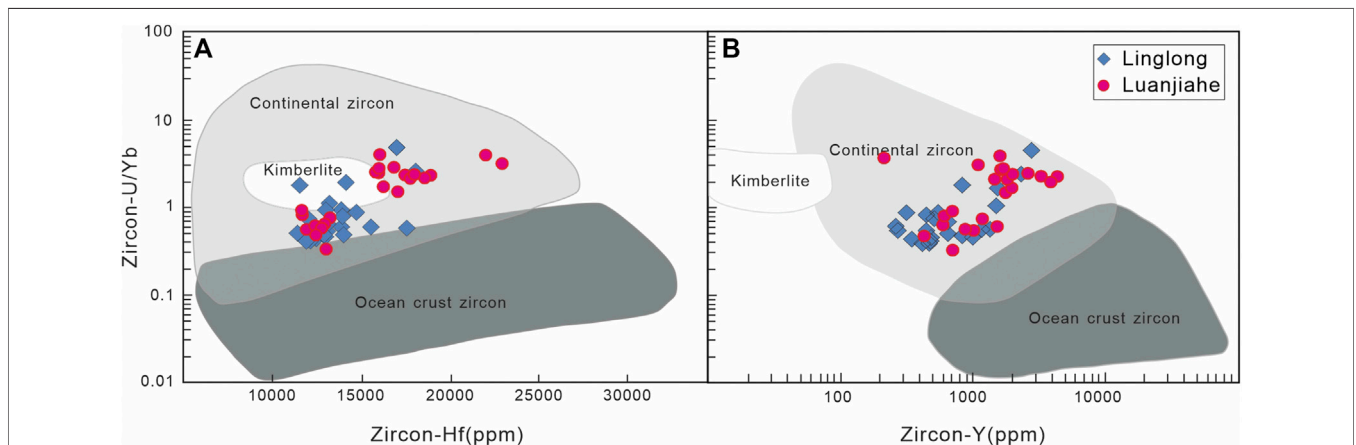


**FIGURE 8 | Zircon Hf vs U/Yb (A)** and Y vs U/Yb **(B)** diagrams for the Linglong and Luanjiahe granites in the Jiabei terrane. The fields of continental and oceanic crust zircon and kimberlite are after Grimes et al. (2007).

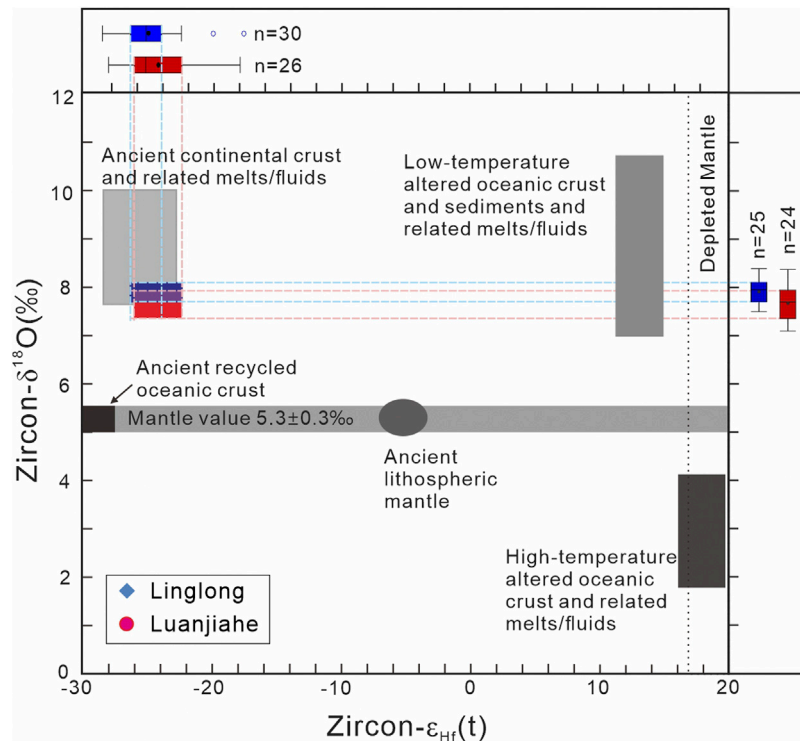


**FIGURE 9** | Zircon  $\epsilon_{\text{Hf}}(t)$  vs  $\delta^{18}\text{O}$  diagram and related box diagrams for the Linglong and Luanjiahe granites. The Hf isotope data are from Yang et al. (2012). Areas of low-temperature altered oceanic crust and sediments and related melts/fluids, high-temperature altered oceanic crust and related melts/fluids, areas of the ancient lithospheric mantle, ancient continental crust, and ancient recycled oceanic crust are referred from Zhu et al. (2017).

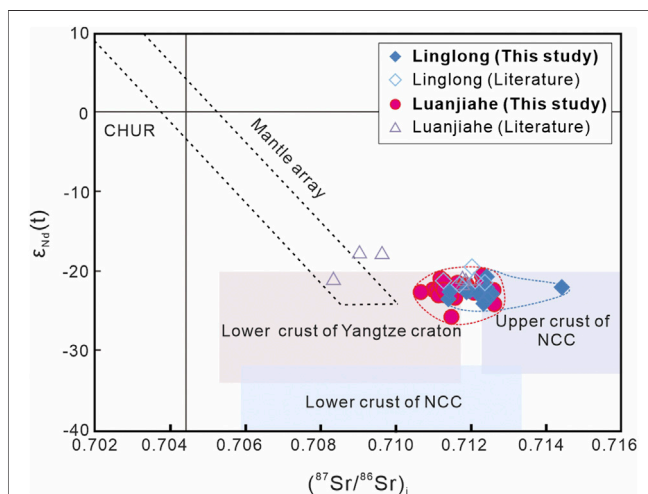


**FIGURE 10** |  $(^{87}\text{Sr}/^{86}\text{Sr})_1$  vs  $\epsilon_{\text{Nd}}(t)$  diagram for the Linglong and Luanjiahe granite. Data sources: the literature data are from Yang et al. (2012); upper and lower crust of the NCC and the Yangtze Craton from Jahn et al. (1999). All the  $(^{87}\text{Sr}/^{86}\text{Sr})_1$  and  $\epsilon_{\text{Nd}}(t)$  values are calculated using the Chondrite Uniform Reservoir (CHUR) values of  $^{87}\text{Rb}/^{86}\text{Sr} = 0.0847$  and  $^{87}\text{Sr}/^{86}\text{Sr} = 0.7045$  ( $\lambda_{\text{Rb}} = 1.42 \times 10^{-11} \text{ year}^{-1}$ ), and  $^{147}\text{Sm}/^{144}\text{Nd} = 0.1967$  and  $^{143}\text{Nd}/^{144}\text{Nd} = 0.512638$  ( $\lambda_{\text{Sm}} = 6.54 \times 10^{-12} \text{ year}^{-1}$ ; Lugmair and Marti, 1978).

The results suggest a similar magma oxidation state for the Linglong and Luanjiahe granites. The  $\text{Ce}^{4+}/\text{Ce}^{3+}$  and oxygen fugacity ( $f\text{O}_2$ ; **Supplementary Table S2**) were calculated using zircon and whole-rock geochemistry data via the methods proposed by Ballard et al. (2002) and Trail et al. (2011). Our calculated results show that the  $\text{Ce}^{4+}/\text{Ce}^{3+}$  ratios of the Linglong and Luanjiahe granites range from 7.05 to 149 (mean 53.1) and 1.08 to 169 (mean 52.2), and the  $f\text{O}_2$  mainly varies from  $-16$  to  $-20$  and  $-15$  to  $-20$  (**Supplementary Table S2**; **Figure 12**), which are consistent with similar oxygen fugacity conditions. Thus, the Linglong and Luanjiahe granite were derived from magma with a similar and moderate oxidation state.

Water can decrease the effective viscosity of the crust and lithospheric mantle of a craton, causing instability of the craton (Arcay et al., 2005; Grant et al., 2007; Peslier et al., 2010; Peslier et al., 2012). Estimating the variation of the water content in magmas is therefore important for investigating craton reworking. Apatite, as a carrier of halogens and water, records the halogen and water fugacity during the cooling and crystallization of the parental magma (Patiño Douce et al., 2011; Gross et al., 2013; Webster and Piccoli, 2015; Pan et al., 2016; Palma et al., 2019). Boyce and Hervig (2009) showed that there was a positive correlation between the variation of OH in

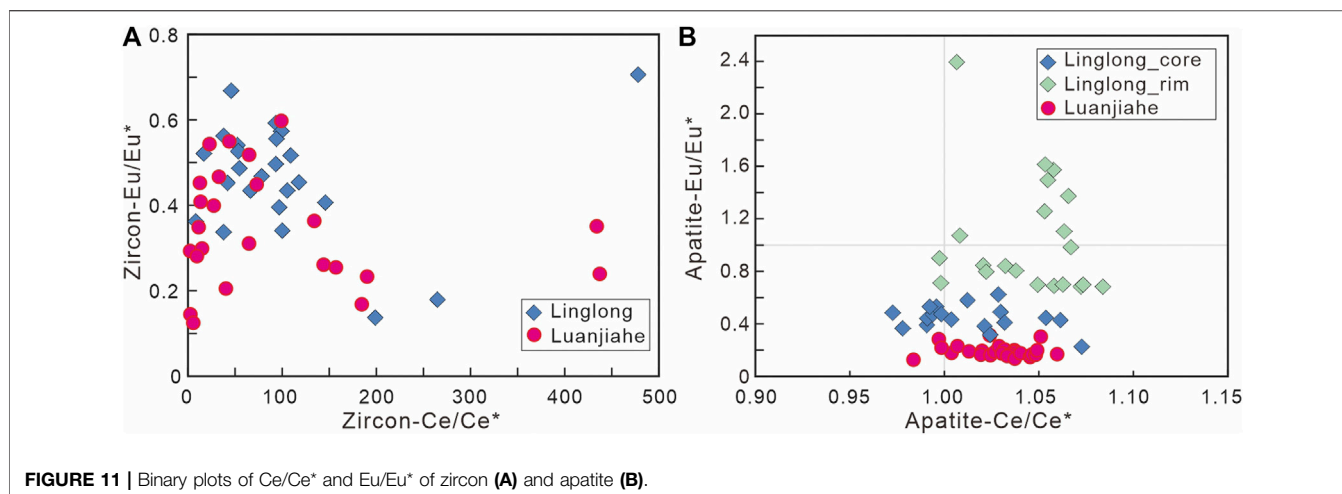


**FIGURE 11** | Binary plots of Ce/Ce\* and Eu/Eu\* of zircon (A) and apatite (B).

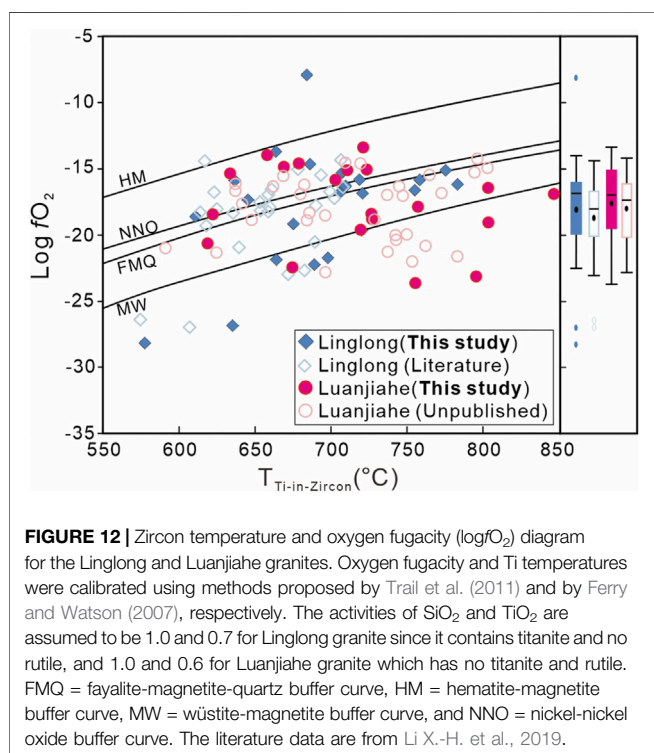


**FIGURE 12** | Zircon temperature and oxygen fugacity ( $\log fO_2$ ) diagram for the Linglong and Luanjiahe granites. Oxygen fugacity and Ti temperatures were calibrated using methods proposed by Trail et al. (2011) and by Ferry and Watson (2007), respectively. The activities of  $SiO_2$  and  $TiO_2$  are assumed to be 1.0 and 0.7 for Linglong granite since it contains titanite and no rutile, and 1.0 and 0.6 for Luanjiahe granite which has no titanite and rutile. FMQ = fayalite-magnetite-quartz buffer curve, HM = hematite-magnetite buffer curve, MW = wüstite-magnetite buffer curve, and NNO = nickel-nickel oxide buffer curve. The literature data are from Li X.-H. et al., 2019.

apatite and  $H_2O$  in the coexisting melt using experimental data for the partitioning behavior of F, Cl, and OH between apatite and the melt. Given the positive correlation, the variation of OH content in apatite has often been used to assess the water fugacity or relative abundance of  $H_2O$  in the melt (e.g., Webster et al., 2009; Cao et al., 2012; Robinson and Taylor, 2014; McCubbin et al., 2015; Pan et al., 2016). Although the absolute  $H_2O$  contents of the magma could not be estimated due to the lack of F or Cl data, Linglong apatite has much higher OH than Luanjiahe apatite (8.2 mol% vs 0.96 mol%; **Figure 7**), indicating a more water-rich parental magma for the Linglong granite. This is

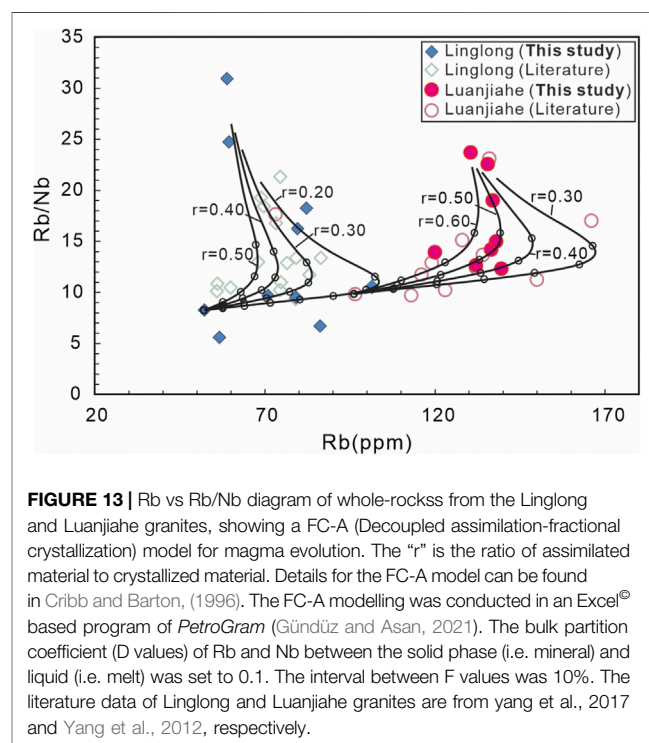


**FIGURE 13** | Rb vs Rb/Nb diagram of whole-rock samples from the Linglong and Luanjiahe granites, showing a FC-A (Decoupled assimilation-fractional crystallization) model for magma evolution. The “r” is the ratio of assimilated material to crystallized material. Details for the FC-A model can be found in Cribb and Barton, (1996). The FC-A modelling was conducted in an Excel® based program of *PetroGram* (Gündüz and Asan, 2021). The bulk partition coefficient (D values) of Rb and Nb between the solid phase (i.e. mineral) and liquid (i.e. melt) was set to 0.1. The interval between F values was 10%. The literature data of Linglong and Luanjiahe granites are from yang et al., 2017 and Yang et al., 2012, respectively.

consistent with the Linglong granites having higher Sr (707–1380 ppm vs 479–665 ppm) and Ba contents (mean 2,376 vs 1,526 ppm; **Supplementary Table S1**), because hydrothermal experiments of You et al. (1996) indicate that Ba and Sr contents in magma are positive correlated with the degree of fluid enrichment. Evidence is also provided by the higher contents of biotite, lower contents of plagioclase, and occurrence of amphibole in Linglong granites (**Figure 2**), because the occurrence of amphibole or biotite phenocrysts is often indicative of high magmatic water concentration, as water promotes amphibole fractionation and suppresses plagioclase crystallization (Davidson et al., 2007; Grove et al., 2012; Richards et al., 2012; Xing et al., 2021). Therefore, the above

observations indicate that the Linglong magmas had higher water contents than Luanjiahe.

### Magma Formation Processes

Previous studies mostly argued for a similar magmatic evolution for the Late Jurassic granites in the Jiaobei terrane (e.g., Jiang N. et al., 2010; Yang et al., 2012; Li H. et al., 2019). However, the differences in textures, mineral assemblages (Figure 2), and mineral geochemistry (Supplementary Tables 4, 5) suggest that they may have been formed by different magma processes.

The observation of local residual basement rocks (e.g., Archean TTG gneisses; Wu X. D. et al., 2020; Wang et al., 2021) and the occurrence of Neoproterozoic, Neoproterozoic, and Triassic inherited zircons in the Linglong and Luanjiahe granites (Supplementary Figure S1) suggests crustal assimilation in the shallow crust. Here we examine the roles of fractional crystallization and assimilation during the formation of the granite by modelling Rb and Rb/Nb data as proposed by Cribb and Barton (1996; Figure 13). They show markedly different Rb contents (Figure 13), combined with the higher F contents of Luanjiahe apatite (Figure 7), reflecting that the Luanjiahe granite is more evolved and richer in volatiles (Supplementary Table S4) since the F and Rb contents are positively correlated with magmatic evolution degree (Ekwere, 1985). The modelling results show that the variations between the Rb and Rb/Nb of the Linglong and Luanjiahe granites are consistent with the decoupled assimilation-fractional crystallization (FC-A) magmatic evolution model at  $r = 0.2\text{--}0.5$  and  $0.3\text{--}0.6$ , respectively (Figure 13). The FC-A model emphasizes that the assimilation and dissociated crystallization process are not fully correlated in a magma system, and the mass of assimilation was separated from the mass of crystallization and varied independently (e.g., Cribb and Barton, 1996; Chen and Arakawa, 2005). In summary, both the Linglong and Luanjiahe granites have undergone different degrees of crustal assimilation and crystal fractionation.

Apatite can separate the trace elements such as REE, Y, Sr, Th, and U in the parent magma during crystallization by various substitution/coupled-substitution reactions (Boudreau and Kruger, 1990; Wolf and London, 1995; Hughes and Rakovan, 2015). The apatite of Linglong granites shows distinct light-dark zoning (Figure 4C), which is usually due to magma mixing or changes in the surrounding magmatic environment (e.g., oxygen fugacity, fluid circulation, magma composition, etc.; Piccoli and Candela, 2002; Streck, 2008; Bruand et al., 2014). A detailed study by Tepper and Kuehner (1999) indicates that magma-mixed apatite often displays a feature of lack systematic core-to-rim chemical variations. Our data show there is a synchronous decrease in REE + Y, Th and U in rims to cores of Linglong apatites (Supplementary Table S5), indicating that the zoning may not be caused by the magmatic mixing. Changes in oxygen fugacity will cause changes in the contents of variable elements with multiple valence states such as Ce and Eu in the magma. The data in this paper show variation in the Eu anomalies between the cores and rims (Figure 11B), which is controlled by the plagioclase crystallization rather than a change in  $fO_2$ . Thus, the simple change in  $fO_2$  cannot explain the abrupt change in REE between cores and rims. Water enrichment may promote the Sr and LREE in magma (You et al., 1996). There is a slightly

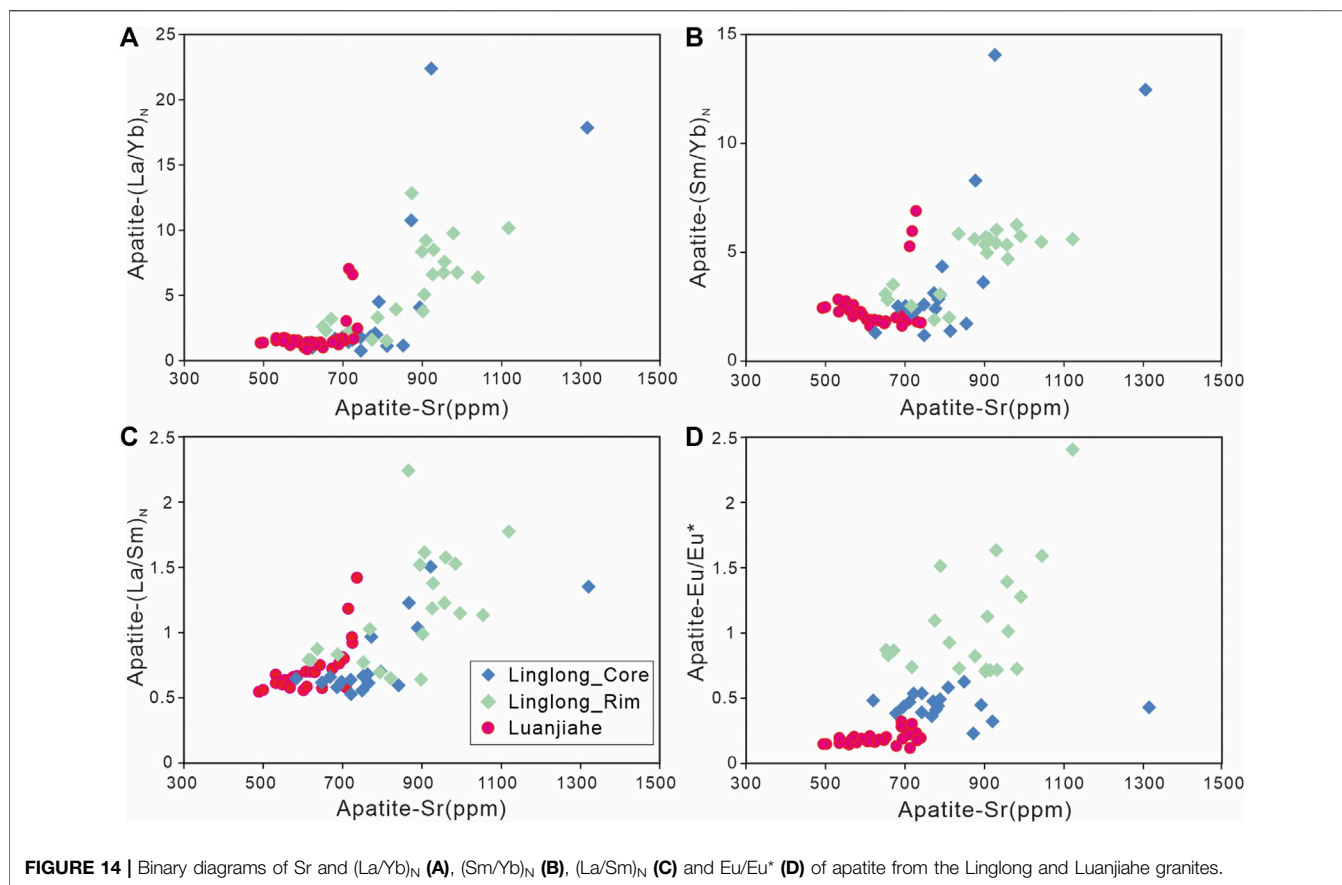
increasing in Sr (866 ppm vs 802 ppm) and  $\Sigma\text{LREE}/\Sigma\text{HREE}$  (5.3 vs 3.3) between the Linglong apatite rims to cores, which may indicate a change in magmatic hydrous environment. The calculating of OH contents shows an increasing trend in the rims compared to the cores of Linglong apatite (Figure 7B), which may indicate an increase in magmatic water contents during the formation of apatite zoning as clarified above. Collectively, the zonation of Linglong apatite may be due to changes in the surrounding magmatic environment likely related to the water contents.

The Sr partitioning is not sensitive to melt composition or temperature (Blundy and Wood, 1989; Du et al., 2019), thus in most cases, the Sr content of apatite is greatly influenced by the crystallization of other Sr-rich minerals (e.g., plagioclase; Wolf and London, 1995; Du et al., 2019; Sun et al., 2022). The REE + Sr variations in apatite, such as the  $(\text{La}/\text{Yb})_N$ ,  $(\text{Sm}/\text{Yb})_N$ ,  $(\text{La}/\text{Sm})_N$  ratios, and Sr contents, closely reflect the mineral crystallization process (e.g., Belousova et al., 2002; Andersson et al., 2019; Zhang et al., 2019). The  $(\text{La}/\text{Yb})_N$ ,  $(\text{Sm}/\text{Yb})_N$ , and  $(\text{La}/\text{Sm})_N$  ratios of Linglong apatite have a significant positive correlation with Sr contents (Figures 14A–C), indicating that the plagioclase crystallization, which preferentially partitions Sr, has a significant influence on the composition of the magma when apatite crystallized. In addition, plagioclase has a strong affinity to host Eu, particularly  $\text{Eu}^{2+}$  (Drake, 1975), and its crystallization can result in Eu depletion (and negative Eu anomalies) in syn- or post-crystallized minerals. The cores of Linglong apatite have more significant negative Eu anomalies than the rims (0.23–0.63 vs 0.70–2.40; Figure 14D), suggesting a greater effect on early-stage Linglong apatite from plagioclase crystallization. In contrast, the enhanced suppression of plagioclase fractionation owing to increasing water contents in the later stage implies a weaker effect of plagioclase fractionation on apatite chemistry, which is consistent with a weak negative to positive Eu anomalies of the apatite rims (Figure 14D).

There are no significant positive correlation between the  $(\text{La}/\text{Yb})_N$ ,  $(\text{Sm}/\text{Yb})_N$ ,  $(\text{La}/\text{Sm})_N$  ratios and Sr contents of Luanjiahe apatite (Figures 14A–C), indicating that plagioclase had less influence on the Luanjiahe magma when apatite crystallized. Compared to the Linglong apatite, the low Sr contents of Luanjiahe apatite (mean 623 vs 837 ppm) and strong negative Eu (0.12–0.32; Figure 14D) anomalies of Luanjiahe apatite could further suggest that plagioclase have crystallized before apatite since the crystallization of plagioclase would separate Sr and Eu from the magma. This is consistent with that the Luanjiahe apatite is subhedral (Figure 4D) and commonly found as an inclusion in quartz (Figure 2I) but not in plagioclase. In addition, there is a strong negative Eu (0.12–0.32) anomaly in the Luanjiahe apatite, which is also likely caused by the crystallization of plagioclase that has separated Eu from the magma. In summary, the early crystallization of plagioclase in the Luanjiahe granite can explain the characteristics of Sr and Eu in apatite.

### Implications for the Geodynamic Setting at Late Jurassic

The petrogenesis of late Jurassic granites in northwest Jiaodong has important implications for the tectonic evolution of the southeast



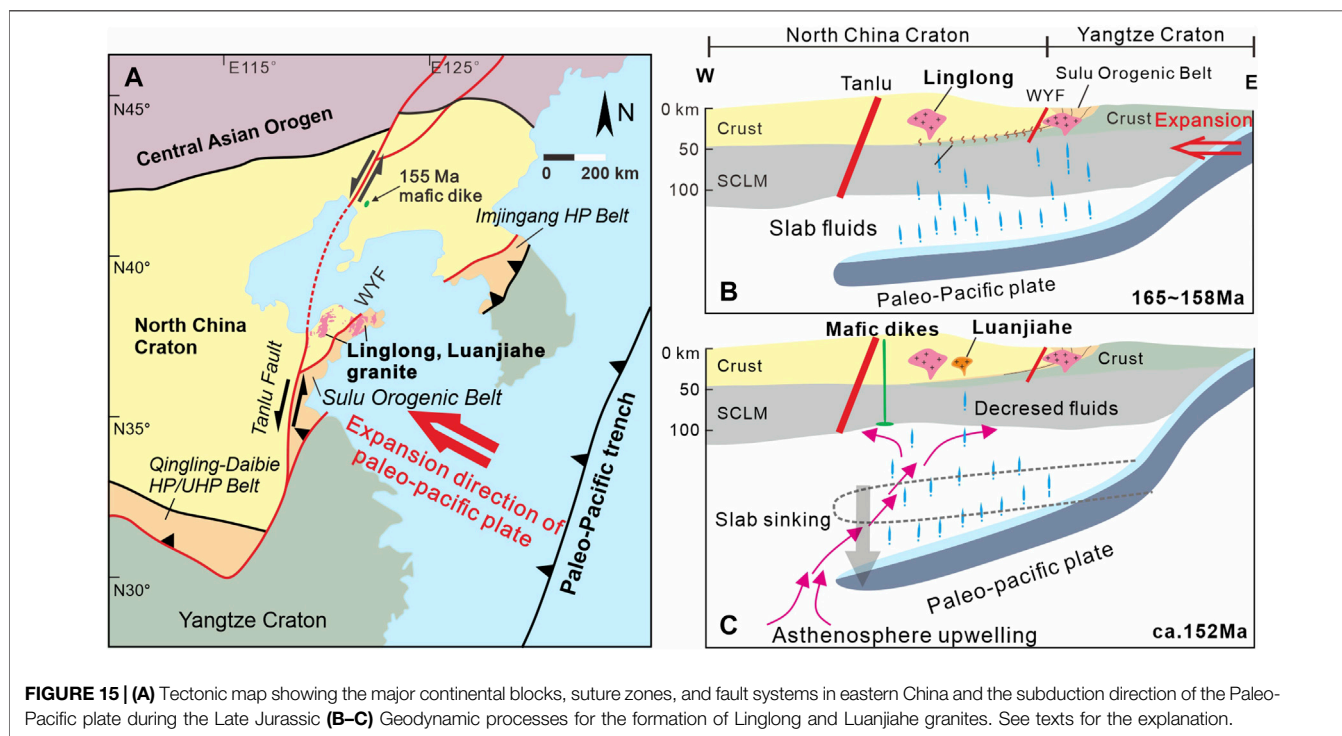
margin of the NCC. Most of the Linglong and Luanjiahe samples have  $Al_2O_3/(CaO + Na_2O + K_2O)$  ratios concentrated between 1.0 and 1.1 consistent with a transitional I-type to S-type origin, whereas some of the Linglong samples have ratios  $<1$  more consistent with an I-type origin (Figure 3B). Whole-rock geochemistry data show that the granites have high Sr (479–1380 ppm), low Yb (0.15–1.06 ppm) and Y (1.70–11.7 ppm) contents, high  $(La/Yb)_N$  (23–260), and Sr/Y (59–600) ratios with only minor Eu anomalies ( $Eu/Eu^*$  mostly in 0.8–1.2), similar to adakitic rocks (Atherton and Petford, 1993; Lai and Qin, 2013). Typically, adakitic rocks form by melting of the thickened mafic lower crust, or in crystal fractionation of normal basaltic arc magmas under high-pressure conditions, or by partial melting of young oceanic crust under eclogitic facies conditions (Atherton and Petford, 1993; Reay and Parkinson, 1997; Tang et al., 2017). The new zircon and apatite chemistry data for the Linglong and Luanjiahe granites are consistent with melting of the thickened mafic lower crust, probably a combination of NCC and Yangtze craton basement, during the Late Jurassic in the Jiaodong Peninsula.

Our zircon geochronology data suggest that the Linglong granite was formed at ca. 158 Ma (Figures 5A,B), which is generally coeval with the sinistral strike-slip (164–156 Ma) along the Tanlu fault based on muscovite  $^{40}Ar/^{39}Ar$  dating of mylonite (Wang, 2006; Wu H. J. et al., 2020). The

contemporaneous granitic magmatism (Figure 1A) and deformation probably indicate that the continuous NW-trending subduction of the paleo-Pacific plate (start at ca. 170 Ma; Liu et al., 2019; Zhu and Xu, 2019) lead both to the thickening of the mafic lower crust and reactivation of the Tanlu fault as a sinistral strike-slip fault (Figure 15A).

The Linglong granite is more widespread than the Luanjiahe granite in the Jiaodong Peninsula (Figure 1A). As discussed above, the source magmas of the Linglong and Luanjiahe granites were both derived from the ancient continental crust, with the parent magma for the Linglong granite (ca. 158 Ma) having higher water contents than the Luanjiahe granite (ca. 152 Ma). Typically, the addition of water can lower the melting temperature and facilitate the partial melting of the thickened underlying crust (e.g., Gaetani and Grove, 1998; Collins et al., 2021). Hence, we infer that more water may resulted in the more extensive formation of the Linglong granite while decreasing water made the limited Luanjiahe granite, that is the water has dominated the formation of Late Jurassic granites.

Magmas derived from partial melting of the lower crust are generally enhanced by the breakdown of amphibole in the lower crust and/or the input of supercritical fluids from the subducting oceanic slab (Kay and Mpodozis, 2002; Reich et al., 2003; Deng et al., 2017). The similar magmatic sources of the Linglong and Luanjiahe granite and the likely low-angle subduction of the Paleo-Pacific slab



(e.g., Deng et al., 2017; Liu et al., 2019; Zhu and Xu, 2019), suggest that the magmatic water originated from the shallow Paleo-Pacific oceanic crust beneath the NCC and Yangtze Craton (Figures 15B,C). The earliest mafic dikes (lamprophyre; ocean-island basalt (OIB) type) in the NCC formed at ca. 155 Ma (Figure 15C) are interpreted to have originated from subcontinental lithospheric mantle driven by asthenospheric upwelling caused by slab roll-back setting (Jiang Y.-H. et al., 2010; Deng et al., 2017; Liu et al., 2019; Liang et al., 2020). The lower water contents of the Luanjiahe magma (Figure 7), suggest that the Paleo-Pacific slab may have begun to sink or roll-back at ca. 155–152 Ma causing a reduced input of associated with water the subducted oceanic crust, due to an increasing distance from the slab to continental crust (Figure 15C). Therefore, we provide new constraints on the geodynamic setting in the Late Jurassic when the Paleo-Pacific plate began to sink or roll-back, likely accompanied by asthenospheric upwelling (e.g., Deng et al., 2017; Liu et al., 2019).

## CONCLUSIONS

This paper presents new geochronological, geochemical, and isotopic data for the Linglong and Luanjiahe granites and related zircon and apatite to investigate the petrogenesis of Late Jurassic granite. Zircon U-Pb dating shows that the Linglong granite emplacement in the Jiabei terrane occurred at ca. 158 Ma, whereas the Luanjiahe granite formed at ca. 152 Ma, consistent with the intrusive contact relationships. The parental magma for the Late Jurassic granites originated from the partial

melting of thickened ancient continental crust (NCC crust and Yangtze crust) and underwent a decoupled assimilation-fractional crystallization process to form the Linglong and Luanjiahe granites. Apatite and zircon geochemistry data indicate the two granites share similar oxygen fugacity, but the parental magma for the Linglong granite contained much more water than Luanjiahe. The above conclusions combined with the subduction setting of the paleo-Pacific plate suggest the occurrence of slab roll-back of a low-angle ocean slab and accompanying asthenospheric upwelling at ca. 155–152 Ma. Such a tectonic transition in the Late Jurassic perhaps represents the initiation of the large-scale NCC reworking, as the prolonged slab roll-back would cause the intense mantle-crust interaction and reduce lithosphere strength and accelerate crustal extension that facilitates lithosphere thinning of the craton.

## DATA AVAILABILITY STATEMENT

The original contributions presented in the study are included in the article/Supplementary Material, further inquiries can be directed to the corresponding author.

## AUTHOR CONTRIBUTIONS

XM and JH conceived of the presented idea. XM, XQ, ZL, PD, and HY did the field investigation and sample collection. XM, XQ, and ZL conducted all the experiments. XM, XQ, and JH wrote the

original draft. ZL and PH reviewed and edited the draft. All authors discussed the results and contributed to the final manuscript.

## FUNDING

This study was jointly funded by the National Natural Science Foundation of China (Nos. 42030809, 41972309, 42072325, and 42172328), the Project of Innovation-driven Plan of Central South University (No. 2020zzts644), Hunan Provincial Innovation Foundation for Postgraduate (No. CX20200112) and the National Key R&D Program of China (No. 2017YFC0601503).

## REFERENCES

- Andersson, S. S., Wagner, T., Jonsson, E., Fusswinkel, T., and Whitehouse, M. J. (2019). Apatite as a Tracer of the Source, Chemistry and Evolution of Ore-Forming Fluids: The Case of the Olserum-Djupedal REE-Phosphate Mineralisation, SE Sweden. *Geochimica Cosmochimica Acta* 255, 163–187. doi:10.1016/j.gca.2019.04.014
- Arcay, D., Tric, E., and Doin, M.-P. (2005). Numerical Simulations of Subduction Zones. *Phys. Earth Planet. Interiors* 149, 133–153. doi:10.1016/j.pepi.2004.08.020
- Atherton, M. P., and Petford, N. (1993). Generation of Sodium-Rich Magmas from Newly Underplated Basaltic Crust. *Nature* 362, 144–146. doi:10.1038/362144a0
- Ballard, J. R., Palin, M. J., and Campbell, I. H. (2002). Relative Oxidation States of Magmas Inferred from Ce(IV)/Ce(III) in Zircon: Application to Porphyry Copper Deposits of Northern Chile. *Contrib. Mineral. Pet.* 144, 347–364. doi:10.1007/s00410-002-0402-5
- Belousova, E. A., Griffin, W. L., O'Reilly, S. Y., and Fisher, N. I. (2002). Apatite as an Indicator Mineral for Mineral Exploration: Trace-Element Compositions and Their Relationship to Host Rock Type. *J. Geochem. Explor.* 76, 45–69. doi:10.1016/S0375-6742(02)00204-2
- Blundy, J. D., and Wood, B. J. (1989). Crystal-chemical Controls on the Partitioning of Sr and Ba between Plagioclase Feldspar, Silicate Melts, and Hydrothermal Solutions. *Geochim. Cosmochim. Acta* 55, 193–209. doi:10.1016/0016-7037(91)90411-W
- Boudreau, A. E., and Kruger, F. J. (1990). Variation in the Composition of Apatite through the Merensky Cyclic Unit in the Western Bushveld Complex. *Econ. Geol.* 85, 737–745. doi:10.2113/gsecongeo.85.4.737
- Boyce, J. W., and Hervig, R. L. (2009). Apatite as a Monitor of Late-Stage Magmatic Processes at Volcán Irazú, Costa Rica. *Contrib. Mineral. Pet.* 157, 135–145. doi:10.1007/s00410-008-0325-x
- Bruand, E., Storey, C., and Fowler, M. (2014). Accessory Mineral Chemistry of High Ba-Sr Granites from Northern Scotland: Constraints on Petrogenesis and Records of Whole-Rock Signature. *J. Pet.* 55, 1619–1651. doi:10.1093/petrology/egu037
- Cao, M., Li, G., Qin, K., Seitmuratova, E. Y., and Liu, Y. (2012). Major and Trace Element Characteristics of Apatites in Granitoids from Central Kazakhstan: Implications for Petrogenesis and Mineralization. *Resour. Geol.* 62, 63–83. doi:10.1111/j.1751-3928.2011.00180.x
- Chen, B., and Arakawa, Y. (2005). Elemental and Nd-Sr Isotopic Geochemistry of Granitoids from the West Junggar Foldbelt (NW China), with Implications for Phanerozoic Continental Growth. *Geochimica Cosmochimica Acta* 69, 1307–1320. doi:10.1016/j.gca.2004.09.019
- Collins, W. J., Murphy, J. B., Blereau, E., and Huang, H.-Q. (2021). Water Availability Controls Crustal Melting Temperatures. *Lithos* 402–403, 106351. doi:10.1016/j.lithos.2021.106351
- Cribb, J. W., and Barton, M. (1996). Geochemical Effects of Decoupled Fractional Crystallization and Crustal Assimilation. *Lithos* 37, 293–307. doi:10.1016/0024-4937(95)00027-5
- Davidson, J., Turner, S., Handley, H., Macpherson, C., and Dosseto, A. (2007). Amphibole “Sponge” in Arc Crust? *Geol* 35, 787–790. doi:10.1130/g23637a.1

## ACKNOWLEDGMENTS

This paper greatly benefited from the constructive comments of three reviewers. Qingling Xiao provides insightful comments for the draft. Mijun Wang and Benhai Ha are appreciated for their assistance during field work.

## SUPPLEMENTARY MATERIAL

The Supplementary Material for this article can be found online at: <https://www.frontiersin.org/articles/10.3389/feart.2022.850440/full#supplementary-material>

- Defant, M. J., and Drummond, M. S. (1990). Derivation of Some Modern Arc Magmas by Melting of Young Subducted Lithosphere. *Nature* 347, 662–665. doi:10.1038/347662a0
- Deng, J., Liu, X., Wang, Q., Dilek, Y., and Liang, Y. (2017). Isotopic Characterization and Petrogenetic Modeling of Early Cretaceous Mafic Diking-Lithospheric Extension in the North China Craton, Eastern Asia. *GSA Bull.* 129, 1379–1407. doi:10.1130/b31609.1
- Deng, J., Qiu, K.-F., Wang, Q.-F., Goldfarb, R., Yang, L.-Q., Zi, J.-W., et al. (2020). *In Situ* Dating of Hydrothermal Monazite and Implications for the Geodynamic Controls on Ore Formation in the Jiaodong Gold Province, Eastern China. *Econ. Geol.* 115, 671–685. doi:10.5382/econgeo.4711
- Drake, M. J. (1975). The Oxidation State of Europium as an Indicator of Oxygen Fugacity. *Geochimica Cosmochimica Acta* 39, 55–64. doi:10.1016/0016-7037(75)90184-2
- Du, J., Wang, G., and Jia, L. (2019). *In Situ* major and Trace Element Compositions of Apatites from Luanchuan Orecluster: Implications for Porphyry Mo Mineralization. *Ore Geol. Rev.* 115, 103174. doi:10.1016/j.oregeorev.2019.103174
- Ekwere, S. J. (1985). Li, F and Rb Contents and Ba/Rb and Rb/Sr Ratios as Indicators of Postmagmatic Alteration and Mineralization in the Granitic Rocks of the Banke and Ririwai Younger Granite Complexes, Northern Nigeria. *Mineral. Deposita* 20, 88–93. doi:10.1007/bf00204315
- Ferry, J. M., and Watson, E. B. (2007). New Thermodynamic Models and Revised Calibrations for the Ti-In-Zircon and Zr-In-Rutile Thermometers. *Contrib. Mineral. Pet.* 154, 429–437. doi:10.1007/s00410-007-0201-0
- Gaetani, G. A., and Grove, T. L. (1998). The Influence of Water on Melting of Mantle Peridotite. *Contributions Mineralogy Petrology* 131, 323–346. doi:10.1007/s004100050396
- Grant, K. J., Kohn, S. C., and Brooker, R. A. (2007). The Partitioning of Water between Olivine, Orthopyroxene and Melt Synthesised in the System Albite-Forsterite-H<sub>2</sub>O. *Earth Planet. Sci. Lett.* 260, 227–241. doi:10.1016/j.epsl.2007.05.032
- Griffin, W. L., Powell, W. J., Pearson, N. J., and O'Reilly, S. Y. (2008). GLITTER: Data Reduction Software for Laser Ablation ICP-MS. *Laser Ablation ICP-MS Earth Sci. Curr. Pract. Outst. issues* 40, 308–311.
- Grimes, C. B., John, B. E., Kelemen, P. B., Mazdab, F. K., Wooden, J. L., Cheadle, M. J., et al. (2007). Trace Element Chemistry of Zircons from Oceanic Crust: A Method for Distinguishing Detrital Zircon Provenance. *Geol* 35, 643–647. doi:10.1130/g23603a.1
- Gross, J., Filiberto, J., and Bell, A. S. (2013). Water in the Martian Interior: Evidence for Terrestrial MORB Mantle-like Volatile Contents from Hydroxyl-Rich Apatite in Olivine-Phyric Shergottite NWA 6234. *Earth Planet. Sci. Lett.* 369–370, 120–128. doi:10.1016/j.epsl.2013.03.016
- Grove, T. L., Till, C. B., and Krawczynski, M. J. (2012). The Role of H<sub>2</sub>O in Subduction Zone Magmatism. *Annu. Rev. Earth Planet. Sci.* 40, 413–439. doi:10.1146/annurev-earth-042711-105310
- Gündüz, M., and Asan, K. (2021). PetroGram: An Excel-Based Petrology Program for Modeling of Magmatic Processes. *Geosci. Front.* 12, 81–92. doi:10.1016/j.gsf.2020.06.010
- Hoskin, P. W. O., and Schaltegger, U. (2003). 2. The Composition of Zircon and Igneous and Metamorphic Petrogenesis. *Rev. Mineralogy Geochem.* 53, 27–62. doi:10.1515/9781501509322-005

- Hou, M.-L., Jiang, Y.-H., Jiang, S.-Y., Ling, H.-F., and Zhao, K.-D. (2007). Contrasting Origins of Late Mesozoic Adakitic Granitoids from the Northwestern Jiaodong Peninsula, East China: Implications for Crustal Thickening to Delamination. *Geol. Mag.* 144, 619–631. doi:10.1017/s0016756807003494
- Hughes, J. M., and Rakovan, J. F. (2015). Structurally Robust, Chemically Diverse: Apatite and Apatite Supergroup Minerals. *Elements* 11, 165–170. doi:10.2113/gselements.11.3.165
- Irvine, T. N., and Baragar, W. R. A. (1971). A Guide to the Chemical Classification of the Common Volcanic Rocks. *Can. J. Earth Sci.* 8, 523–548. doi:10.1139/e71-055
- Jahn, B.-m., Wu, F., Lo, C.-H., and Tsai, C.-H. (1999). Crust-mantle Interaction Induced by Deep Subduction of the Continental Crust: Geochemical and Sr-Nd Isotopic Evidence from Post-collisional Mafic-Ultramafic Intrusions of the Northern Dabie Complex, Central China. *Chem. Geol.* 157, 119–146. doi:10.1016/s0009-2541(98)00197-1
- Jiang, N., Guo, J. H., Zhai, M. G., and Zhang, S. Q. (2010a). 2.7 Ga Crust Growth in the North China Craton. *Precambrian Res.* 179, 27–49. doi:10.1016/j.precamres.2010.02.010
- Jiang, Y.-H., Jiang, S.-Y., Ling, H.-F., and Ni, P. (2010b). Petrogenesis and Tectonic Implications of Late Jurassic Shoshonitic Lamprophyre Dikes from the Liaodong Peninsula, NE China. *Min. Pet.* 100, 127–151. doi:10.1007/s00710-010-0124-8
- Kay, S. M., and Mpodozis, C. (2002). Magmatism as a Probe to the Neogene Shallowing of the Nazca Plate beneath the Modern Chilean Flat-Slab. *J. S. Am. Earth Sci.* 15, 39–57. doi:10.1016/s0895-9811(02)00005-6
- Kusky, T. M., Windley, B. F., and Zhai, M.-G. (2007). Tectonic Evolution of the North China Block: from Orogen to Craton to Orogen. *Geol. Soc. Lond. Spec. Publ.* 280, 1–34. doi:10.1144/sp280.1
- Lai, S.-c., and Qin, J.-f. (2013). Adakitic Rocks Derived from the Partial Melting of Subducted Continental Crust: Evidence from the Eocene Volcanic Rocks in the Northern Qiangtang Block. *Gondwana Res.* 23, 812–824. doi:10.1016/j.gr.2012.06.003
- Li, H., Sun, H.-S., Evans, N. J., Li, J.-W., Wu, J.-H., Jiang, W.-C., et al. (2019a). Geochemistry and Geochronology of Zircons from Granite-Hosted Gold Mineralization in the Jiaodong Peninsula, North China: Implications for Ore Genesis. *Ore Geol. Rev.* 115, 103188. doi:10.1016/j.oregeorev.2019.103188
- Li, X.-H., Fan, H.-R., Hu, F.-F., Hollings, P., Yang, K.-F., and Liu, X. (2019b). Linking Lithospheric Thinning and Magmatic Evolution of Late Jurassic to Early Cretaceous Granitoids in the Jiaobei Terrane, Southeastern North China Craton. *Lithos* 324–325, 280–296. doi:10.1016/j.lithos.2018.11.022
- Li, X., Li, W., Wang, X., Li, Q., Liu, Y., and Tang, G. (2009). Role of Mantle-Derived Magma in Genesis of Early Yanshanian Granites in the Nanling Range, South China: *In Situ* Zircon Hf-O Isotopic Constraints. *Sci. China Ser. D-Earth Sci.* 52, 1262–1278. doi:10.1007/s11430-009-0117-9
- Li, Z., Duan, D., Jiang, S., Ma, Y., and Yuan, H. (2018). *In Situ* Analysis of Major Elements, Trace Elements and Sr Isotopic Compositions of Apatite from the Granite in the Chengchao Skarn-type Fe Deposit, Edong Ore District: Implications for Petrogenesis and Mineralization. *J. Earth Sci.* 29, 295–306. doi:10.1007/s12583-018-0837-x
- Liang, Y., Liu, X., Wang, Q., Zhao, R., and Ma, Y. (2020). Late Mesozoic Magmatism in the Jiaodong Peninsula, East China: Implications for Crust-Mantle Interactions and Lithospheric Thinning of the Eastern North China Craton. *Geosci. Front.* 11, 895–914. doi:10.1016/j.gsf.2019.09.008
- Liu, J., Cai, R., Pearson, D. G., and Scott, J. M. (2019). Thinning and Destruction of the Lithospheric Mantle Root beneath the North China Craton: A Review. *Earth-Science Rev.* 196, 102873. doi:10.1016/j.earscirev.2019.05.017
- Liu, Z., Hollings, P., Mao, X., Lawley, C. J. M., Yang, B., and Tang, L. (2021). Metal Remobilization from Country Rocks into the Jiaodong-type Orogenic Gold Systems, Eastern China: New Constraints from Scheelite and Galena Isotope Results at the Xiadian and Majiayao Gold Deposits. *Ore Geol. Rev.* 134, 104126. doi:10.1016/j.oregeorev.2021.104126
- Lugmair, G. W., and Marti, K. (1978). Lunar Initial  $^{143}\text{Nd}/^{144}\text{Nd}$ : Differential Evolution of the Lunar Crust and Mantle. *Earth Planet. Sci. Lett.* 39, 349–357. doi:10.1016/0012-821x(78)90021-3
- Ma, L., Jiang, S.-Y., Dai, B.-Z., Jiang, Y.-H., Hou, M.-L., Pu, W., et al. (2013). Multiple Sources for the Origin of Late Jurassic Linglong Adakitic Granite in the Shandong Peninsula, Eastern China: Zircon U-Pb Geochronological, Geochemical and Sr-Nd-Hf Isotopic Evidence. *Lithos* 162–163, 251–263. doi:10.1016/j.lithos.2013.01.009
- Maniar, P. D., and Piccoli, P. M. (1989). Tectonic Discrimination of Granitoids. *Geol. Soc. Am. Bull.* 101, 635–643. doi:10.1130/0016-7606(1989)101<0635:tdog>2.3.co;2
- Mathez, E. A., and Webster, J. D. (2005). Partitioning Behavior of Chlorine and Fluorine in the System Apatite-Silicate Melt-Fluid. *Geochimica Cosmochimica Acta* 69, 1275–1286. doi:10.1016/j.gca.2004.08.035
- McCubbin, F. M., Vander Kaaden, K. E., Tartèse, R., Klima, R. L., Liu, Y., Mortimer, J., et al. (2015). Magmatic Volatiles (H, C, N, F, S, Cl) in the Lunar Mantle, Crust, and Regolith: Abundances, Distributions, Processes, and Reservoirs. *Am. Mineralogist* 100, 1668–1707. doi:10.2138/am-2015-4934ccbyncnd
- Menzies, M. A., Fan, W., and Zhang, M. (1993). Palaeozoic and Cenozoic Lithoprobates and the Loss of >120 Km of Archaean Lithosphere, Sino-Korean Craton, China. *Geol. Soc. Lond. Spec. Publ.* 76, 71–81. doi:10.1144/gsl.sp.1993.076.01.04
- Palma, G., Barra, F., Reich, M., Valencia, V., Simon, A. C., Vervoort, J., et al. (2019). Halogens, Trace Element Concentrations, and Sr-Nd Isotopes in Apatite from Iron Oxide-Apatite (IOA) Deposits in the Chilean Iron Belt: Evidence for Magmatic and Hydrothermal Stages of Mineralization. *Geochimica Cosmochimica Acta* 246, 515–540. doi:10.1016/j.gca.2018.12.019
- Pan, L.-C., Hu, R.-Z., Wang, X.-S., Bi, X.-W., Zhu, J.-J., and Li, C. (2016). Apatite Trace Element and Halogen Compositions as Petrogenetic-Metallogenic Indicators: Examples from Four Granite Plutons in the Sanjiang Region, SW China. *Lithos* 254–255, 118–130. doi:10.1016/j.lithos.2016.03.010
- Patiño Douce, A. E., Roden, M. F., Chaumba, J., Fleisher, C., and Yagodinski, G. (2011). Compositional Variability of Terrestrial Mantle Apatites, Thermodynamic Modeling of Apatite Volatile Contents, and the Halogen and Water Budgets of Planetary Mantles. *Chem. Geol.* 288, 14–31.
- Peslier, A. H., Woodland, A. B., Bell, D. R., Lazarov, M., and Lapen, T. J. (2012). Metasomatic Control of Water Contents in the Kaapvaal Cratonic Mantle. *Geochimica Cosmochimica Acta* 97, 213–246. doi:10.1016/j.gca.2012.08.028
- Peslier, A. H., Woodland, A. B., Bell, D. R., and Lazarov, M. (2010). Olivine Water Contents in the Continental Lithosphere and the Longevity of Cratons. *Nature* 467, 78–81. doi:10.1038/nature09317
- Piccoli, P. M., and Candela, P. A. (2002). 6. Apatite in Igneous Systems. *Rev. Mineral. Geochem.* 48, 255–292. doi:10.1515/9781501509636-009
- Reay, A., and Parkinson, D. (1997). Adakites from Solander Island, New Zealand. *N. Z. J. Geol. Geophys.* 40, 121–126. doi:10.1080/00288306.1997.9514746
- Reich, M., Parada, M. A., Palacios, C., Dietrich, A., Schultz, F., and Lehmann, B. (2003). Adakite-like Signature of Late Miocene Intrusions at the Los Pelambres Giant Porphyry Copper Deposit in the Andes of Central Chile: Metallogenic Implications. *Miner. Deposita* 38, 876–885. doi:10.1007/s00126-003-0369-9
- Ren, J. C. (2017). *Tectonic Facies Characteristics of Coarse - Grained Granoditic Granites in Luanjiahe Type in Jiaodong Northwestern (Master Thesis)*. Beijing: China Univ. Geosci, 1–47. (in Chinese with English abstract).
- Richards, J. P., Spell, T., Rameh, E., Raziq, A., and Fletcher, T. (2012). High Sr/Y Magmas Reflect Arc Maturity, High Magmatic Water Content, and Porphyry Cu ± Mo ± Au Potential: Examples from the Tethyan Arcs of Central and Eastern Iran and Western Pakistan. *Econ. Geol.* 107, 295–332. doi:10.2113/econgeo.107.2.295
- Robinson, K. L., and Taylor, G. J. (2014). Heterogeneous Distribution of Water in the Moon. *Nat. Geosci.* 7, 401–408. doi:10.1038/ngeo2173
- Rudnick, R. L., Gao, S., Ling, W.-l., Liu, Y.-s., and McDonough, W. F. (2004). Petrology and Geochemistry of Spinel Peridotite Xenoliths from Hannuoba and Qixia, North China Craton. *Lithos* 77, 609–637. doi:10.1016/j.lithos.2004.03.033
- Scott, J. A. J., Humphreys, M. C. S., Mather, T. A., Pyle, D. M., and Stock, M. J. (2015). Insights into the Behaviour of S, F, and Cl at Santiaguito Volcano, Guatemala, from Apatite and Glass. *Lithos* 232, 375–394. doi:10.1016/j.lithos.2015.07.004
- Streck, M. J. (2008). 15. Mineral Textures and Zoning as Evidence for Open System Processes. *Rev. Mineral. Geochem.* 69, 595–622. doi:10.1515/9781501508486-016
- Sun, C.-Y., Cawood, P. A., Xu, W.-L., Zhang, X.-M., Tang, J., Li, Y., et al. (2022). *In Situ* geochemical Composition of Apatite in Granitoids from the Eastern Central Asian Orogenic Belt: A Window into Petrogenesis. *Geochimica Cosmochimica Acta* 317, 552–573. doi:10.1016/j.gca.2021.10.028

- Sun, S.-s., and McDonough, W. F. (1989). Chemical and Isotopic Systematics of Oceanic Basalts: Implications for Mantle Composition and Processes. *Geol. Soc. Lond. Spec. Publ.* 42, 313–345. doi:10.1144/gsl.sp.1989.042.01.19
- Tan, J., Wei, J., Audétat, A., and Pettke, T. (2012). Source of Metals in the Guocheng Gold Deposit, Jiaodong Peninsula, North China Craton: Link to Early Cretaceous Mafic Magmatism Originating from Paleoproterozoic Metasomatized Lithospheric Mantle. *Ore Geol. Rev.* 48, 70–87. doi:10.1016/j.oregeorev.2012.02.008
- Tang, G. J., Wang, Q., Wyman, D. A., Chung, S. L., Chen, H. Y., and Zhao, Z. H. (2017). Genesis of Pristine Adakitic Magmas by Lower Crustal Melting: A Perspective from Amphibole Composition. *J. Geophys. Res. Solid Earth* 122, 1934–1948. doi:10.1002/2016jb013678
- Tang, H., Zheng, J., Yu, C., Ping, X., and Ren, H. (2014). Multistage Crust-Mantle Interactions during the Destruction of the North China Craton: Age and Composition of the Early Cretaceous Intrusions in the Jiaodong Peninsula. *Lithos* 190–191, 52–70. doi:10.1016/j.lithos.2013.12.002
- Tepper, H. J., and Kuehner, S. M. (1999). Complex Zoning in Apatite from the Idaho Batholith: A Record of Magma Mixing and Intracrystalline Trace Element Diffusion. *Am. Mineral.* 84, 584–591. doi:10.2138/am-1999-0412
- Trail, D., Tailby, N. D., Lanzirotti, A., Newville, M., Thomas, J. B., and Watson, E. B. (2015). Redox Evolution of Silicic Magmas: Insights from XANES Measurements of Ce Valence in Bishop Tuff Zircons. *Chem. Geol.* 402, 77–88. doi:10.1016/j.chemgeo.2015.02.033
- Trail, D., Watson, E. B., and Tailby, N. D. (2011). The Oxidation State of Hadean Magmas and Implications for Early Earth's Atmosphere. *Nature* 480, 79–82. doi:10.1038/nature10655
- Wang, R., Liu, Z., Hollings, P., Zhou, X., Guo, Y., Li, B., et al. (2020). Fluid Evolution of the Humedo Porphyry-Related Gold Deposit, Southern Ecuador: Evidence from the Boron Isotope and Chemical Variations of Tourmaline. *Ore Geol. Rev.* 128, 103894. doi:10.1016/j.oregeorev.2020.103894
- Wang, Y. (2006). The Onset of the Tan?Lu Fault Movement in Eastern China: Constraints from Zircon (SHRIMP) and <sup>40</sup>Ar/<sup>39</sup>Ar Dating. *Terra. nova.* 18, 423–431. doi:10.1111/j.1365-3121.2006.00708.x
- Wang, Z., Xu, Z., Cheng, H., Zou, Y., Guo, J., Liu, Y., et al. (2021). Precambrian Metamorphic Crustal Basement Cannot Provide Much Gold to Form Giant Gold Deposits in the Jiaodong Peninsula, China. *Precambrian Res.* 354. doi:10.1016/j.precamres.2020.106045
- Webster, J. D., and Piccoli, P. M. (2015). Magmatic Apatite: A Powerful, yet Deceptive, Mineral. *Elements* 11, 177–182. doi:10.2113/gselements.11.3.177
- Webster, J. D., Tappen, C. M., and Mandeville, C. W. (2009). Partitioning Behavior of Chlorine and Fluorine in the System Apatite-Melt-Fluid. II: Felsic Silicate Systems at 200MPa. *Geochimica Cosmochimica Acta* 73, 559–581. doi:10.1016/j.gca.2008.10.034
- Wolf, M. B., and London, D. (1995). Incongruent Dissolution of REE- and Sr-Rich Apatite in Peraluminous Granitic Liquids; Differential Apatite, Monazite, and Xenotime Solubilities during Anatexis. *Am. Mineralogist* 80, 765–775. doi:10.2138/am-1995-7-814
- Wu, F., Lin, J., Wilde, S., Zhang, X., and Yang, J. (2005). Nature and Significance of the Early Cretaceous Giant Igneous Event in Eastern China. *Earth Planet. Sci. Lett.* 233, 103–119. doi:10.1016/j.epsl.2005.02.019
- Wu, H. J., He, Y. S., Li, S. G., Zhu, C. W., and Hou, Z. H. (2020a). Partial Melts of Intermediate-Felsic Sources in a Wedged Thickened Crust: Insights from Granites in the Sulu Orogen. *J. Pet.* 61, 1–35. doi:10.1093/ptrology/egaa053
- Wu, X. D., Zhu, G., Yin, H., Su, N., Lu, Y. C., Zhang, S., et al. (2020b). Origin of Low-Angle Ductile/Brittle Detachments: Examples from the Cretaceous Linglong Metamorphic Core Complex in Eastern China. *Tectonics* 39, e06132. doi:10.1029/2020tc006132
- Xing, K., Shu, Q., and Lentz, D. R. (2021). Constraints on the Formation of the Giant Daheishan Porphyry Mo Deposit (NE China) from Whole-Rock and Accessory Mineral Geochemistry. *J. Pet.* 62, 1–26. doi:10.1093/ptrology/egab018
- Yang, J.-H., Wu, F.-Y., Wilde, S. A., Belousova, E., and Griffin, W. L. (2008a). Mesozoic Decratonization of the North China Block. *Geol.* 36, 467–470. doi:10.1130/g24518a.1
- Yang, K.-F., Fan, H.-R., Santosh, M., Hu, F.-F., Wilde, S. A., Lan, T.-G., et al. (2012). Reactivation of the Archean Lower Crust: Implications for Zircon Geochronology, Elemental and Sr-Nd-Hf Isotopic Geochemistry of Late Mesozoic Granitoids from Northwestern Jiaodong Terrane, the North China Craton. *Lithos* 146–147, 112–127. doi:10.1016/j.lithos.2012.04.035
- Yang, L.-Q., Dilek, Y., Wang, Z.-L., Weinberg, R. F., and Liu, Y. (2017). Late Jurassic, High Ba-Sr Linglong Granites in the Jiaodong Peninsula, East China: Lower Crustal Melting Products in the Eastern North China Craton. *Geol. Mag.* 155, 1040–1062. doi:10.1017/s0016756816001230
- Yang, Y. H., Wu, F. Y., Xie, L. W., Yang, J. H., and Zhang, Y. B. (2009). In-situ Sr Isotopic Measurement of Natural Geological Samples by LA-MC-ICP-MS. *Acta Pet. Sin.* 25, 3431–3441.
- Yang, Y., Sun, J., Xie, L., Fan, H., and Wu, F. (2008b). In Situ Nd Isotopic Measurement of Natural Geological Materials by LA-MC-ICPMS. *Sci. Bull.* 53, 1062–1070. doi:10.1007/s11434-008-0166-z
- Zhai, M., Cong, B., Guo, J., Liu, W., Li, Y., and Wang, Q. (2000). Sm-Nd Geochronology and Petrography of Garnet Pyroxene Granulites in the Northern Sulu Region of China and Their Geotectonic Implication. *Lithos* 52, 23–33. doi:10.1016/s0024-4937(99)00082-1
- Zhai, M., Fan, Q., Zhang, H., Sui, J., and Shao, J. A. (2007). Lower Crustal Processes Leading to Mesozoic Lithospheric Thinning beneath Eastern North China: Underplating, Replacement and Delamination. *Lithos* 96, 36–54. doi:10.1016/j.lithos.2006.09.016
- Zhang, C.-C., Sun, W.-D., Wang, J.-T., Zhang, L.-P., Sun, S.-J., and Wu, K. (2017). Oxygen Fugacity and Porphyry Mineralization: A Zircon Perspective of Dexing Porphyry Cu Deposit, China. *Geochimica Cosmochimica Acta* 206, 343–363. doi:10.1016/j.gca.2017.03.013
- Zhang, H.-F. (2012). Destruction of Ancient Lower Crust through Magma Underplating beneath Jiaodong Peninsula, North China Craton: U-Pb and Hf Isotopic Evidence from Granulite Xenoliths. *Gondwana Res.* 21, 281–292. doi:10.1016/j.gr.2011.05.013
- Zhang, J., Zhao, Z.-F., Zheng, Y.-F., and Dai, M. (2010b). Postcollisional Magmatism: Geochemical Constraints on the Petrogenesis of Mesozoic Granitoids in the Sulu Orogen, China. *Lithos* 119, 512–536. doi:10.1016/j.lithos.2010.08.005
- Zhang, R. W., Xue, C. D., Xue, L. P., and Liu, X. (2019). The Geochemical Characteristics and Their Geological Significance of Apatite from the Bengge Gold Deposit in Sanjiang Region, SW China. *Acta Pet. Sin.* 35, 1407–1422.
- Zhao, R., Wang, Q., Liu, X., Wang, W., and Pan, R. (2016). Architecture of the Sulu Crustal Suture between the North China Craton and Yangtze Craton: Constraints from Mesozoic Granitoids. *Lithos* 266–267, 348–361. doi:10.1016/j.lithos.2016.10.018
- Zhu, R.-X., Yang, J.-H., and Wu, F.-Y. (2012). Timing of Destruction of the North China Craton. *Lithos* 149, 51–60. doi:10.1016/j.lithos.2012.05.013
- Zhu, R., and Xu, Y. (2019). The Subduction of the West Pacific Plate and the Destruction of the North China Craton. *Sci. China Earth Sci.* 62, 1340–1350. doi:10.1007/s11430-018-9356-y
- Zhu, Y.-S., Yang, J.-H., Sun, J.-F., and Wang, H. (2017). Zircon Hf-O Isotope Evidence for Recycled Oceanic and Continental Crust in the Sources of Alkaline Rocks. *Geology* 45, 407–410. doi:10.1130/g38872.1

**Conflict of Interest:** Author PD and HY are employed by Zhaojin Mining Industry Co., Ltd.

The remaining authors declare that the research was conducted in the absence of any commercial or financial relationships that could be construed as a potential conflict of interest.

**Publisher's Note:** All claims expressed in this article are solely those of the authors and do not necessarily represent those of their affiliated organizations, or those of the publisher, the editors and the reviewers. Any product that may be evaluated in this article, or claim that may be made by its manufacturer, is not guaranteed or endorsed by the publisher.

Copyright © 2022 Mao, Qu, Liu, Huang, Hollings, Du and Yang. This is an open-access article distributed under the terms of the Creative Commons Attribution License (CC BY). The use, distribution or reproduction in other forums is permitted, provided the original author(s) and the copyright owner(s) are credited and that the original publication in this journal is cited, in accordance with accepted academic practice. No use, distribution or reproduction is permitted which does not comply with these terms.